Applied Energy 338 (2023) 120945

Contents lists available at ScienceDirect

Applied Energy

journal homepage: www.elsevier.com/locate/apenergy

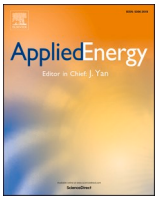

Hydrogen-powered refrigeration system for environmentally friendly transport and delivery in the food supply chain

F. Segura, F.J. Vivas *, J.M. Andújar, M. Martínez

Research Centre on Technology, Energy and Sustainability (CITES), University of Huelva, Spain

HIGHLIGHTS

- APU system for refrigerated light trucks based on hydrogen technology.
- Integral solution based on BoP, power, control and acquisition electronics, control loops.
- Step-by-step design of acquisition, control, and power electronics.
- Validation of experimental performance on refrigerated light truck.
- Proven performance of the proposed solution in terms of autonomy, cost reduction and CO_2 emissions.

ARTICLE INFO

Keywords:
Refrigerated light trucks and vans
Air-cooled PEM fuel cell
Hydrogen-powered refrigeration system
Refrigerated food transport sector
Energy management system

ABSTRACT

Urban population and the trend towards online commerce leads to an increase in delivery solution in cities. The growth of the transport sector is very harmful to the environment, being responsible for approximately 40% of greenhouse gas emissions in the European Union. The problem is aggravated when transporting perishable foodstuffs, as the vehicle propulsion engine (VPE) must power not only the vehicle but also the refrigeration unit. This means that the VPE must be running continuously, both on the road and stationary (during delivery), as the cold chain must be preserved. The result is costly (high fuel consumption) and harmful to the environment. At present, refrigerated transport does not support full-electric solutions, due to the high energy consumption required, which motivates the work presented in this article. It presents a turnkey solution of a hydrogen-powered refrigeration system (HPRS) to be integrated into standard light trucks and vans for short-distance food transport and delivery. The proposed solution combines an air-cooled polymer electrolyte membrane fuel cell (PEMFC), a lithium-ion battery and low-weight pressurised hydrogen cylinders to minimise cost and increase autonomy and energy density. In addition, for its implementation and integration, all the acquisition, power and control electronics necessary for its correct management have been developed. Similarly, an energy management system (EMS) has been developed to ensure continuity and safety in the operation of the electrical system during the working day, while maximizing both the available output power and lifetime of the PEMFC. Experimental results on a real refrigerated light truck provide more than 4 h of autonomy in intensive intercity driving profiles, which can be increased, if necessary, by simply increasing the pressure of the stored hydrogen from the current 200 bar to whatever is required. The correct operation of the entire HPRS has been experimentally validated in terms of functionality, autonomy and safety; with fuel savings of more than 10% and more than 3650 kg of CO_2/year avoided.

1. Introduction

At the beginning of the millennium, the rural population was 1,16 times the urban population. In fact, the rural population has been above the urban population since 1960, when historical data are available [1]. But this trend was reversed in 2007 [2], when the urban population was 50% of the total world population, and by 2050 the urban population is expected to reach 68%. Urbanization will be one of the most transformative trends of the 21st century. With the increase of the world population and the general improvement of living conditions, the demand for food, water and energy is expected to increase by 50%, 30%

* Corresponding author.
E-mail address: francisco.vivas@diesia.uhu.es (F.J. Vivas).

https://doi.org/10.1016/j.apenergy.2023.120945
Received 2 June 2022; Received in revised form 24 February 2023; Accepted 5 March 2023
Available online 13 March 2023

Nomenclature

Acronyms

AC	Alternating Current
APU	Auxiliary Power Unit
BoP	Balance of Plant
CCM	Continuous Conduction Mode
DC	Direct current
EMI	Electromagnetic Interference
EMS	Energy Management System
EU	European Union
FC	Fuel Cell
GHG	Greenhouse Gases
HPRS	Hydrogen-powered refrigeration system
LCV	Light Commercial Vehicles
MPP	Maximum Power Point
P&OM	Modified Perturbation and Observation
PEM	Polymer Electrolyte Membrane
PEMFC	Polymer Electrolyte Membrane Fuel Cell
PWM	Pulse Width Modulation
RS	Refrigeration system
SOC	State of Charge
SOFC	Solid Oxide Fuel Cell
VARS	Vapour Absorption Refrigerated System
VPE	Vehicle propulsion engine

Notation and symbols

C	Filter capacitor (F)
C_{Bat}	Battery capacity (Ah)
$C_{H2_{FC}}$	PEMFC hydrogen consumption rate (litres/min)
δ	Duty cycle
$\Delta I_L(t)$	Inductor ripple current (A)
$\Delta V_C(t)$	Capacitor ripple voltage (V)
E_{req}	Required energy to guarantee the electric compressor operation (Wh)
η_{DCAC}	DC/AC converter performance
η_{H_2}	Hydrogen utilization efficiency of hydrogen-based power system
f_S	PWM signal frequency (20 kHz)
H_2	Hydrogen level (%)
$H_{2_{min}}$	Minimum hydrogen level (%)
$I_C(t)$	Capacitor current (A)
$I_L(t)$	Inductor current (A)
$I_R(t)$	Load current (A)
L	Inductor (H)
P_{H2}	Hydrogen storage pressure (bar)
P_{aux}	Power demanded by auxiliaries (W)
P_{Bat}	Battery power (W)
P_{cool}	Power demanded by the electric refrigeration compressor (W)
P_{DCAC}	DC/AC converter power (W)
P_{DCDC}	Interleaved DC/DC boost converter power (W)
P_{FC}	Fuel cell power (W)
$P_{FC_{SP}}$	Fuel cell preset power limit (V)
R	Load resistor (Ω)
SOC	Battery state of charge (%)
t_{stop}	Daily time when the vehicle stops, and the electric refrigeration compressor activates (h)
T_{amb}	Ambient temperature (°C)
T_{DCDC}	Operating temperature of the DC/DC boost power converter (°C)
$T_{DCDC_{max}}$	Maximum operating temperature allowed at DC/DC boost power converter (°C)
V_{Bat}	Battery voltage (V)
$V_{Bat_{FC}}$	Battery preset voltage to activate fuel cell (V)
$V_{Bat_{min}}$	Minimum battery voltage (V)
$V_{Bat_{max}}$	Maximum battery voltage (V)
V_{Bat_N}	Nominal battery voltage (V)
$V_{DC_{Bus}}$	DC bus voltage (V)
V_{bottle}	Bottle volume (litres)
V_{FC}	Fuel cell voltage (V)
$V_{FC_{SP}}$	Fuel cell preset voltage limit (V)
$V_{H_{2_{bottle}}}$	Volume of hydrogen stored in bottle (litres)
$V_{H_{2req}}$	Required hydrogen volume (litres)
$V_C(t)$	Capacitor voltage (V)
$V_L(t)$	Inductor voltage (V)
Z	Hydrogen compressibility factor

and 45%, respectively [3]. The increase in food demand, as well as the expansion of online commerce, will be accompanied by a proportional growth of food transportation, usually refrigerated. However, the transport sector is one of the most polluting, in Spain for example, in 2019, it reached 29.1% of greenhouse gases (GHG) emissions [4].

In particular, light trucks and vans used for a wide range of services, such as construction, refrigerated food delivery and ambulances [5,6], are responsible for 2.5% of total carbon dioxide (CO_2) emissions in the European Union (EU) [7].

On the other hand, the cold chain, which guarantees the quality and safety of food during transport and delivery, is maintained by means of refrigeration systems (RSs) integrated into vehicles. These cooling systems, whether electric or mechanical, are always powered by a combustion (diesel) engine. The same combustion engine that powers light trucks and vans, or an auxiliary combustion engine in large trucks. Therefore, transport vehicles equipped with RSs consume more fuel and emit more GHG. The environmental impact of a diesel-powered RS can be up to 40% of that of the vehicle propulsion engine (VPE) [8]. The additional diesel consumption due to RS is around 12%, which represents a fuel cost of 6,000 € per year, approximately 40% of the direct cost [9].

Considering the above, refrigerated transport is recognised as one of the main processes in terms of potential energy savings and reduction of GHG emissions in cold chains [10]. The replacement of diesel-based RS by electric (not driven by the VPE) is a strong recommendation for the coming years [11].

In this context, the European Parliament [12] has set an average CO_2 emission target of 147 g CO_2/km for new light commercial vehicles (LCVs) registered in the EU between 2020 and 2024. Spain has a fleet of around 2.5 million LCVs [13], and its target is to reduce emissions by 27 Mt CO_2 by 2030, [14].

In the search for alternative solutions to polluting diesel transport, the need to migrate from internal combustion engines to electric propulsion technology is evident [15]. Currently, the technology is almost exclusively focused on the use of battery-based solutions, but in recent years there has been a great interest in the use of hydrogen-based systems for use in mobile applications [16]. This type of solution is already technically feasible today, characterised by higher energy density compared to battery-based solutions, which is crucial in applications where autonomy and weight reduction are key parameters [16]. In this line of research, few authors have conducted studies on the application of FCs to refrigerated transport.

One of the most recent research focuses on the coupling of a solid oxide FC (SOFC) with a vapour absorption refrigeration system (VARS). The operation is based on the concept of cogeneration, where the heat produced during the operation of the SOFC is used through the VARS to

cool the isothermal refrigerated box, while the generated electricity can be used to meet the consumption of the RS and the vehicle auxiliaries when the VPE is off. Examples of these architectures are studied at simulation level in [3] and [17]. Specifically, in [3] the feasibility of series–parallel SOFC + VARS assembly configurations for use in small, medium and large vans or trucks is analysed from a thermal-economic point of view. A similar study is developed in [17], where the behaviour and technical feasibility of a SOFC auxiliary power unit (APU) with a NH_3 - H_2O based VARS is modelled, simulated and analysed.

The drawback of using SOFCs, [3] and [17], is that they are high temperature FCs (750–1000 °C that require a preheating stage, which lasts up to several tens of minutes [16]. In addition to the above, the operation of SOFCs requires a complex balance of plant (BoP) and energy management system (EMS) that considers the necessary thermal and electrical requirements [18]. Apart from this, SOFCs are designed to provide at least several tens of kilowatts, so they are oversized for use in light refrigerated trucks and vans. Finally, it would require additional space and specific thermal conditions in the vehicle that are difficult to achieve. In contrast, polymer electrolyte membrane fuel cells (PEMFCs) are available from several watts to tens of kilowatts, with smaller size and weight than SOFCs for the same power [19]. Compared to SOFC, PEMFC is characterized by a simpler BoP, a shorter start-up and shutdown times (in the range of seconds), a lower operating temperature (around 70 °C), as well as a better dynamic response [20], which makes it ideal for use in applications such as the one studied here.

Probably, based on the above, other authors have considered the use of PEMFCs for RSs in vehicles. At the simulation level, a comparative study of different hybrid system architectures based on batteries and hydrogen (PEMFCs), for application in a refrigerated semi-trailer truck, is presented in [21]. The performance of each configuration in terms of efficiency and weight was evaluated by simulation for a 60-hour trip. Similarly, in [9] a hybrid power system based on batteries and PEMFC for use in refrigerated trucks is simulated, designed and modelled using the SH2&FC software tool. The scope of this work ends with a techno-economic feasibility analysis based on system sizing and different consumption profiles, as well as a hydrogen chain availability study. Prototype testing is postponed for future work.

Several papers have evaluated experimental prototypes. For example, [22] proposes a hybrid architecture based on supercapacitors, batteries and a PEMFC as APU to power the electric RS replacing the vehicle's internal 12 VDC battery and alternator. In this architecture, the supercapacitors absorb the power peaks during the RS starts, while the PEMFC supplies the demand profile the rest of the time. The role of the battery is to ensure the power supply to the BoP of the PEMFC. Although the prototype shows its technical feasibility, successive changes in operating power, as well as repetitive on/off cycling of the PEMFC will lead to its rapid degradation, with the consequent loss of performance, efficiency and economic unfeasibility [23]. Moreover, its validation was carried out at the laboratory level, so the integration of the APU in the vehicle is not addressed.

Similarly, a hybrid architecture based on batteries and a multi-stack PEMFC system, composed of three PEMFCs operating in parallel, is presented in [24]. The function of the prototype is to replace the auxiliary diesel engine that powers the compressor of refrigerated semi-trailer trucks with a hydrogen-powered genset. The sizing of the system follows the roles defined for the batteries and the PEMFCs. In this case, the batteries are used as a short-term energy storage system (with a small-capacity battery), while the hydrogen system is used for the long term (with a large-capacity H_2 tank). Experimental tests include individual component characterization and RS validation for different temperature conditions simulated in a climatic chamber. Despite the experimental nature of this work, its performance has only been evaluated during the so-called pulldown phase, in which the RS operates at maximum power to reach the target temperature, so no information is available on the performance of the RS in the temperature regulation phase. In addition, vehicle integration and road testing are not addressed.

Finally, Nuvera® presents in [25] a proprietary prototype of a high-power hybrid architecture for use in long-haul refrigerated trucks. The proposal aims to replace the RS auxiliary diesel engine with a solution that integrates the hybrid system and the RS in the same chassis. A 20 kW PEMFC is used to power the electric RS on a 480 VAC bus. In this case, the prototype developed for commercial purposes has closed dimensions and power ratings, which makes it impossible to be adapted to different vehicle sizes and applications, in addition to requiring structural changes in the vehicle for installation.

In response to the shortcomings found in the literature, the authors present in this work a turnkey solution of a hydrogen-powered refrigeration system (HPRS) that, fully integrated in light trucks and vans, allows transporting and delivering refrigerated goods in an environmentally friendly way.

To the authors' knowledge, neither a detailed design demonstrating the full integration of this type of RS in a vehicle, nor experimental results tested under real driving profiles, have been published in the scientific literature so far. The proposed solution is based on a "plug and play" philosophy that hybridizes an air-cooled PEMFC with a lithium-ion battery pack and pressurized lightweight hydrogen bottles.

The main novelties of the proposal presented in this paper are listed below:

- The developed HPRS minimizes cost and increases autonomy and energy density.
- The developed EMS ensures continuity and safety in the operation of the whole RS and vehicle facilities.
- The developed EMS extends the lifetime and maximizes the power extracted from the PEMFC under intensive intercity driving profiles.
- The developed HPRS is easily integrated into the commercial chassis of light trucks and vans without the need for structural changes.
- The vehicle's original RS, both in terms of equipment and facilities, remains unchanged.
- The performance of the developed HRPS has been validated in experimental road tests under intensive intercity driving profiles.

Table 1 presents a comparative between the reviewed literature and the authors' proposal.

The paper is organized as follows: Section 2 explains the materials and methods used to develop the HPRS, including a detailed description of the design, power electronics and EMS. Section 3 brings together the physical implementation and experimental results, which are discussed in Section 4. Finally, conclusions are presented in Section 5.

2. Materials and methods

The definition and design of the proposed HPRS is based on the energy requirements defined for the practical application under study. Specifically, the HPRS has been designed for integration and use in a light truck for the transport of refrigerated perishable food at a temperature of 4 °C in an 8-hour intercity driven profile. The scenario is a city in south-western Spain (Huelva) with a subtropical climate and, therefore, with many cold losses in transport and delivery. The driven profile is characterized by a high number of short distance trips followed by a high number of stops to unload goods. Specifically, for the current design of the HPRS, driving and stopping times of the vehicle have been considered similar (4 h driving on the road and 4 h in standby or parked), according to estimates and surveys of professionals in the sector.

The following sections will present the design of the architecture and components of the developed HPRS.

Table 1
Comparison of the contributions of the work presented with the literature reviewed.

Reference	Fuel Cell	Manufacturer	Nominal Power	Feature	Powered by	Development level
Authors proposal	PEMFC	Horizon®	2 kW	Conservative use of hydrogen. Enhanced lifespan. Thermal control of the hydrogen system. P&OM* control algorithm for PEMFC. Range extender application. Autonomy:4 h extendable to more than 8 h.	PEMFC + batteries	Full integration on vehicle. Prototype on the road
[3]	SOFC	Non detailed	Small van: 3.3 kW Medium van: 12.8 kW Large van: 18.7 kW	The SOFC powers the electrical part, and its waste heat powers the VARS	VARS + SOFC	Simulation
[17]	SOFC	Non detailed	Small van: 2 kW Medium van: 5 kW Large van: 9 kW	Separates the cooling load from the main diesel engine	VARS + SOFC	Simulation
[21]	PEMFC	Non detailed	Non detailed	Analysis of architectures for a hybrid FC and battery power supply. Comparison of hydrogen consumption and degradation	PEMFC + batteries	Simulation
[9]	PEMFC	Non detailed	–	Analysis of load profiles. Study of hydrogen chain	PEMFC + batteries	Simulation
[22]	PEMFC	Ballard Power System®	1.2 kW	Hydrogen-based APU powers the cooling electrical load by replacing battery and alternator	PEMFC + batteries	Laboratory set-up
[24]	PEMFC	Non detailed	Non detailed	Replaces the fuel tank and the diesel engine driving the cooling compressor with a hydrogen-powered genset	PEMFC + batteries	Laboratory set-up
[25]	PEMFC	Nuvera®	20 kW	FC-based APU prototype. Component characterization	PEMFC + batteries	Laboratory testing of individual components

* Modified perturbation and observation algorithm to extract the maximum power from the PEMFC.

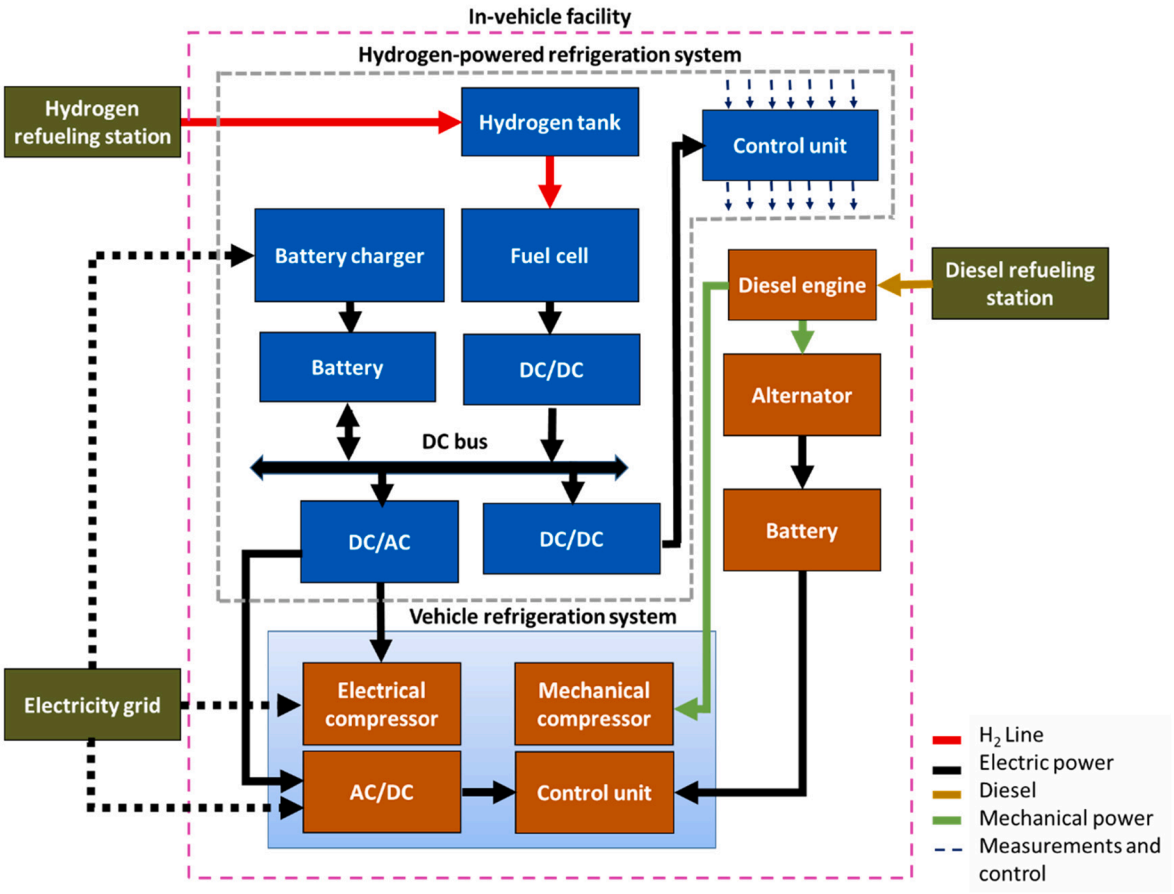

Fig. 1. Vehicle-integrated hydrogen-powered refrigeration system architecture.

2.1. Design and sizing

2.1.1. Hydrogen-powered refrigeration system architecture

To meet the desired objective, the HRPS architecture must be properly designed. To this end, it is essential to take advantage of all the standard equipment of the vehicle to minimize the modifications to be made. This will facilitate the homologation of the vehicle after its upgrade and, on the other hand, will make the diesel-hydrogen conversion cheaper.

In this regard, it is common for refrigerated light trucks and vans to integrate two complementary solutions to operate the RS. The first is based on the use of a mechanical compressor, mechanically coupled to the VPE (larger refrigerated trucks have an auxiliary diesel engine to power the RS), Fig. 1. Logically, this configuration only works when the VPE is on. The second is based on a three-phase AC or single-phase AC electric unit, which includes an electric compressor. This means that when the vehicle is at a service station or base, the RS can be powered from the electricity grid through a socket provided in the vehicle, Fig. 1.

Considering the premise of easy integration, the HPRS design is based on the existing electrical unit. For this purpose, two energy storage systems, battery, and hydrogen, will be hybridized. From this starting point, a power electronic and control system will be implemented which, together with the development of a specific EMS, must ensure a constant supply of the RS. Therefore, the conceived solution is that when the vehicle is running, the mechanical compressor driven by the VPE will power the RS. However, when the vehicle is parked or stopped for delivery, the VPE will be turned off, and the HPRS will be responsible for maintaining the RS through the vehicle's electric compressor.

The proposed HPRS architecture is based on the design of a hybrid system consisting of a battery, the hydrogen subsystem, a DC bus, all the necessary power and control electronics, and the EMS (housed in the control unit) that manages everything, Fig. 1.

The HPRS battery sets the DC bus voltage and remains permanently charged through it. Therefore, the function of the FC is to recharge the battery by supplying power to the DC bus through its DC/DC converter, which converts the unregulated power at the output of the FC into regulated power at the DC bus. The vehicle's electric compressor is powered from the DC bus through a DC/AC converter that also powers the RS control unit. The HPRS is completed with the hydrogen storage tank and the necessary supply lines, solenoid and control valves, and pressure regulation devices. In addition, a standard battery charger has been incorporated to charge the HPRS battery from the electricity grid. Thus, in case of FC failure or lack of hydrogen, the HPRS can continue to operate with reduced autonomy.

2.1.2. HPRS energy requirements

The energy required by the HPRS is determined by the described intercity route of the vehicle. Thus, considering the rated power of the installed electric refrigeration compressor (P_{cool} = 2.5 kW), the overall stopping time (t_{stop} = 4 h) and the DC/AC conversion efficiency, η_{DCAC}, estimated at 90 %, equation (1) determines the required amount of energy (E_{req}) to be supplied by the HPRS during a working day. The worst-case scenario has been considered, i.e., the compressor is always running during the stopping time.

$$E_{req} = \frac{P_{cool} \cdot t_{stop}}{\eta_{DCAC}} \tag{1}$$

Resulting E_{req} = 11.11 kWh.

2.1.3. Fuel cell and hydrogen storage sizing

- Fuel cell sizing

The PEMFC chosen is an air-cooled FC, due to its reduced BoP, lower cost and easy management [26–28]. Regarding its sizing, it must respond to a commitment between energy and power. Thus, it will not be necessary to use a FC whose power is at least equal to the maximum power required, which would considerably increase its cost. As shown in Fig. 1, the battery is directly connected to the DC bus, so it can support the maximum power. However, the FC should charge the battery quickly (when the vehicle is in motion and the electric compressor is off) and contribute efficiently to avoid large battery discharges during stopping times.

Considering the solutions available on the market and design considerations, the Horizon® 2000 W air-cooled PEMFC was chosen. This model integrates the entire BoP and its control, which greatly facilitates the integration and management tasks. For the purposes of this research, the FC is a black box through which hydrogen enters and unregulated electrical power exits.

- Hydrogen storage sizing

For the sizing of the hydrogen storage system, it is necessary to consider the autonomy of the HPRS, as well as certain physical limitations in terms of weight and dimensions. The weight should be as low as possible so as not to reduce the vehicle's payload capacity too much. In terms of size, the ideal is to take advantage of the vehicle's structural openings, avoiding any modifications of its chassis.

Based on the above, it has been decided to use pressurized hydrogen bottles of low weight and small dimensions, specially designed for mobile applications. Taking into account the solutions available on the market, the required autonomy and the design considerations, the Carbotainer® B20 200 bar (full weight 25 kg, dimensions: Ø 30 mm and length 900 mm) has been selected. This bottle is made of lightweight materials, such as high-performance carbon fiber and thermoplastic polymers, which give it high mechanical strength. In addition, the aluminium alloy coating (thin metallic layer that prevents the passage of hydrogen) has undergone a heat treatment that makes it highly elastic and resistant to fatigue cycles, giving it a service lifespan of 30 years.

Once the hydrogen bottle has been selected, it is necessary to calculate the number of units needed to guarantee the required autonomy of the HPRS.

For this, knowing the rated power (P_{FC}) and hydrogen consumption ($C_{H2_{FC}}$) of the selected PEMFC, 2000 W and 1560 L/h (26 l/min) respectively, and considering a conservative energy use of hydrogen (η_{H_2}) of 80 % (due to losses associated with the efficiency of the DC/DC converter, wiring, protections and purges), the overall volume of hydrogen needed to guarantee the required autonomy of the HPRS ($V_{H_{2req}}$) corresponds to expression (2).

$$V_{H_{2req}} = \frac{E_{req} \bullet 50\%}{P_{FC} \bullet \eta_{H_2}} \bullet C_{H2_{FC}} \tag{2}$$

Resulting $V_{H_{2req}}$ = 5417 L.

Knowing the volume (V_{bottle} = 20 L) and operating pressure of the selected bottle (P_{H_2} = 200 bar), and considering the hydrogen compressibility factor (Z = 1,132 at 200 bar and 298 K), the total volume of hydrogen available in the bottle ($V_{H_{2\_bottle}}$) is calculated in equation (3):

$$V_{H_{2_{bottle}}} = \frac{V_{bottle} \bullet P_{H_2}}{Z} \tag{3}$$

Resulting $V_{H_{2_{bottle}}}$ = 3534 L.

Therefore, two bottles will be required to keep the proposed HPRS in operation during vehicle stopping time for a full working day.

2.1.4. Battery sizing

Several fundamental aspects have been considered for the sizing of the battery, such as energy density, commercial availability, nominal voltage, and autonomy.

As already discussed, one of the key aspects is the minimization of the weight of the HPRS. This is critical to maximize the payload of the vehicle. This requires the use of high energy density battery technology, so lithium-ion technology batteries will be used for this application.

The choice of rated battery voltage is closely linked to the commercial availability of both batteries and DC/AC converters. Specifically, the most common commercial solutions, and therefore more robust and economical, are based on battery configurations covering voltage ranges from 12 to 72 VDC, the most common being 12, 24, 48 and 60 VDC. The selection of the nominal voltage of the battery must respond to a commitment between the availability of commercial solutions and operation at low currents, as this reduces costs in losses, wiring and electrical protection. Based on the above, a battery with a nominal voltage (V_{Bat_N}) of 60 VDC has been chosen.

Finally, the battery autonomy is determined by calculating its nominal capacity (C_{Bat}). Then, considering the energy to be provided by the battery (50 % of (1)), its nominal voltage ($V_{BatN} = 60$ VDC), as well as the power supply of the BoP and all the developed electronics ($P_{aux} =$ 350 W approximately), the value of its nominal capacity is defined by expression (4).

$$C_{Bat} = \frac{E_{req} \bullet 50\% + P_{aux} \cdot t_{stop}}{V_{BatN}} \tag{4}$$

Resulting $C_{Bat} = 116$ Ah.

Based on the calculations performed, a commercial Samsung® 50E battery of 60 VDC and 120 Ah has been chosen.

2.1.5. DC/DC boost converter design

For the correct integration and control of the PEMFC on the DC bus, defined by the selected battery, and considering their nominal voltage values ($V_{FC} = 28$ VDC, $V_{Bat_N} = 60$ VDC), it is evident the need to use a boost topology power converter, specifically with a boost ratio of approximately 2:1. Such a ratio is easily achievable with the use of non-isolated topologies [29,30], which are simpler and cheaper than isolated ones, and which also operate in a practically linear region and with high efficiency. Specifically, for this application and for the selected PEMFC, the use of a 2-kW interleaved boost DC/DC converter is proposed. The use of an interleaved architecture allows reducing the design requirements of the power components, increasing the overall converter efficiency by reducing Joule losses when operating at lower currents, as well as reducing the current ripple at the converter input, which is essential to reduce stress in the PEMFC operation [31,32]. Specifically, the interleaved DC/DC boost converter consists of two DC/DC boost converters operating in parallel with analog control signals 180° out of phase with each other.

Finally, to complement the positive effect of the interleaved topology with respect to the PEMFC output current ripple, as well as to reduce electromagnetic interference (EMI) and its impact on the rest of the electronics, a PI-type EMI filter has been used at the input of each converter. Fig. 2 shows the architecture of the proposed interleaved boost converter.

- DC/DC boost converter model

For the design of the interleaved DC/DC boost converter it is necessary to obtain the mathematical model describing its behaviour. To simplify the analysis, it is sufficient to evaluate the dynamic behaviour of a single DC/DC boost converter, since the operation of both converters is analogous and independent. For its modelling, the operation in continuous conduction mode (CCM) will be considered.

For modelling purposes, the components will be ideal (this is sufficient for this analysis). Two characteristic times, t_{off} and t_{on}, will be defined, representing the fractions of time in which the MOSFET transistor Q is OFF (case 1) and ON (case 2) respectively. The sum of both times defines the period T of the control signal. According to the above, the equivalent circuit of the DC/DC boost converter for cases 1 and 2 is

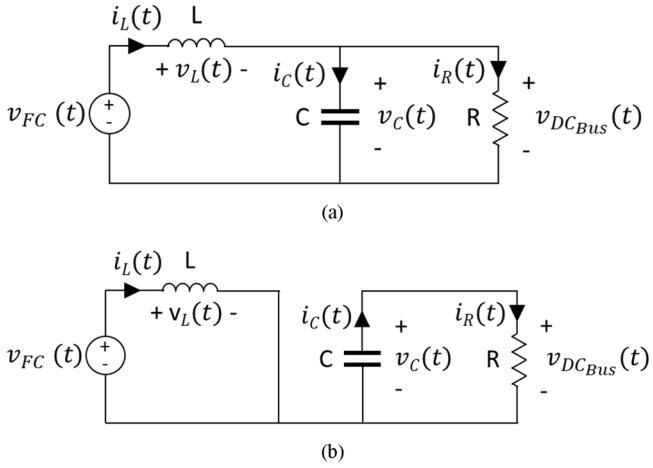

Fig. 3. DC/DC boost converter. a) Equivalent circuit for Q off, case 1; b) Equivalent circuit for Q on, case 2.

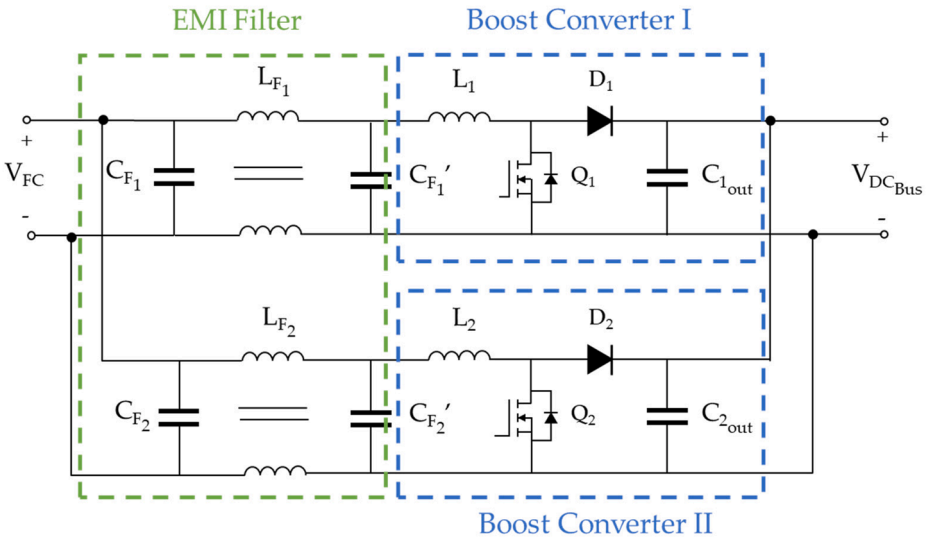

Fig. 2. Interleaved DC/DC boost converter.

shown in Fig. 3a and 3b respectively.

Considering case 1, Fig. 3a. Q is OFF, D is forward biased and thus drives the current from the PEMFC to the output of the DC/DC converter, Fig. 3a. Then, assuming a constant input and output voltage, V_{FC} and $V_{DC_{Bus}}$ due to the FC and the high capacitance capacitor C and the battery, the voltage at L is also constant and negative, $v_L(t) = V_{FC} - V_{DC_{Bus}}$, and the current through L decreases linearly. Based on above, and according to the equivalent circuit of Fig. 3a, the equations modelling the current and voltage behaviour of the of the capacitor and inductor are presented in (5) and (6) respectively.

$$i_C(t) = C\frac{dv_C(t)}{dt} = i_L(t) - i_R(t) \rightarrow \frac{dv_C(t)}{dt} = \frac{i_L(t)}{C} - \frac{v_C(t)}{RC} \tag{5}$$

$$v_L(t) = L\frac{di_L(t)}{dt} = v_{FC}(t) - v_C(t) \rightarrow \frac{di_L(t)}{dt} = \frac{v_{FC}(t) - v_C(t)}{L} \tag{6}$$

On the other hand, when Q is ON (case 2, Fig. 3b), regardless of the abrupt transition of the electronic switch, the inductor current must maintain continuity, so D is reversed biased, Fig. 3b. Then, assuming a constant input voltage V_{FC} due to the FC, the voltage at L is also constant and positive, $v_L(t) = V_{FC}$, and the current at L increases linearly. Based on the above, and according to the equivalent circuit in Fig. 3b, the equations modelling the current and voltage behaviour of the capacitor and inductor are presented in Eqs. (7) and (8) respectively.

$$i_C(t) = C\frac{dv_C(t)}{dt} = -i_R(t) \rightarrow \frac{dv_C(t)}{dt} = -\frac{v_C(t)}{RC} \tag{7}$$

$$v_L(t) = L\frac{di_L(t)}{dt} = v_{FC}(t) \rightarrow \frac{di_L(t)}{dt} = \frac{v_{FC}(t)}{L} \tag{8}$$

Considering the inductor current and capacitor voltage as state variables, the FC voltage $v_{FC}(t)$ as input variable, the DC bus voltage as output variable and considering the duty cycle, $\delta = t_{on}/T$, equations (5) - (8) allow to obtain the state space model of the converter (9). For the instantaneous value of the converter model, the duty cycle takes values of 1 and 0 during the time intervals t_{on} and t_{off}, respectively, coinciding with the practical limit of the duty cycle of the transistor. For the average value of the model, the duty cycle takes values between 0 and 1, coinciding with the duty cycle of the converter.

$$\begin{bmatrix} \dot{i}_L \\ \dot{v}_C \end{bmatrix} = \begin{bmatrix} 0 & -\frac{(1-\delta)}{L} \\ \frac{(1-\delta)}{C} & -\frac{1}{RC} \end{bmatrix} \begin{bmatrix} i_L \\ v_C \end{bmatrix} + \begin{bmatrix} \frac{1}{L} \\ 0 \end{bmatrix} [v_{FC}]$$

$$[v_{DC_{Bus}}] = [0 \quad 1] \begin{bmatrix} i_L \\ v_C \end{bmatrix} \tag{9}$$

The DC/DC converter transfer function can be calculated from the model developed in (9) for the steady state ($\left[\dot{i}_L \dot{v}_C\right]^T = 0$), resulting in equation (10).

$$\frac{V_{DC_{Bus}}}{V_{FC}} = \frac{1}{1-\delta} \tag{10}$$

Eq. (10) shows that by varying the duty cycle it is possible to regulate the conversion ratio.

- DC/DC Boost Converter design and implementation

For the design of the inductance and capacitance of each boost converter, its operation in CCM will be considered and therefore the expressions (5)-(8) and (10). The design characteristics in terms of power, conversion ratio and frequency of the control signal will be established as follows.

Considering the power required and the advantages of the interleaved topology, each DC/DC boost converter should provide half the current/power of the entire DC/DC boost converter, i.e., 1 kW.

For the calculation of the conversion ratio, it is necessary to define the worst-case condition in the PEMFC – DC bus connection through the converter. Then, if the FC always works at its nominal power, $V_{FC} = 28$ VDC; however, the DC bus voltage can reach a maximum value of 64 VDC due to its direct connection to the battery. Based on the above, and according to (10), the duty cycle responding to the most restrictive condition will be $\delta = 0.563$.

Finally, to govern the switching of the transistors of the converter, a pulse width modulation (PWM) signal frequency (f_S) of 20 kHz has been selected because is value widely used in power electronics design.

For the inductor calculation, based on Fig. 3b, when Q is ON, the relationship between current and the voltage at L is given by (8) and in its incremental form by (11).

$$\frac{\Delta I_L}{\Delta t} = \frac{V_L}{L} = \frac{V_{FC}}{L} \tag{11}$$

If $\Delta t = t_{on} = \delta/f_S$, (11) can be written as (12).

$$L = \frac{V_{FC} \bullet \delta}{\Delta I_L \bullet f_S} \tag{12}$$

Since ΔI_L is the swing of the current in the inductor L during t_{on}, in practice, it is the ripple. However, (12) shows that the price to pay for a low ripple is a large inductor, which may be a bad decision, because as is well known the most non-ideal element of the converter is precisely the inductor. Therefore, it is best to assume a relatively large ripple in the inductor which can then be damped by a high capacitance output capacitor. Thus, assuming a conservative value $\Delta I_L = 30\% \bullet I_L$ and using the extreme values in (12), the value of L is obtained by (13).

$$L = \frac{28VDC \bullet 0.563}{0.3 \bullet \frac{1000W}{28VDC} \bullet 20000Hz} = 74\mu\text{H} \tag{13}$$

Therefore, a commercial 80 μH inductor is chosen.

Regarding the output capacitor C, according to Fig. 3b, its voltage is given by (7), and in its incremental form by (14).

$$\frac{\Delta V_C}{\Delta t} = \frac{I_C}{C} \tag{14}$$

Again, if $\Delta t = t_{on} = \delta/f_S$, C is given by (15).

$$C = \frac{I_C \bullet \delta}{\Delta V_C \bullet f_S} \tag{15}$$

Where I_C will be that corresponding to the ripple in L, $I_C = \Delta I_L = 30\% \bullet I_L$. Thus, assuming a voltage variation at the output voltage of only $1\% \bullet V_{DC_{Bus}}$ (this will keep $V_{DC_{Bus}}$ constant, as desirable), and using, again, extreme values, the C value is obtained by (16).

$$C = \frac{0.3 \cdot \frac{1000W}{28VDC} \cdot 0.563}{0.01 \cdot 64VDC \cdot 20000Hz} = 470\mu F \tag{16}$$

Therefore, a commercial 470 μF capacitor is chosen.

2.2. Development

Based on the sizing performed in Section 2.1 and the general structure of the HPRS presented in Fig. 1, this section will develop in detail the proposed HPRS, which is shown in Fig. 4.

The HPRS architecture is composed of three systems, the power unit, the hydrogen storage, and the cabin control, which integrates the ignition key and the user interface, each of them located in a different area of the truck according to its functionality. Thus, the power unit is located inside the refrigerated box of the vehicle, inside a thermally insulated enclosure specially designed for this application (blue area, Fig. 4). The choice of this location responds to two fundamental needs, space, and cooling. As this is a prototype of HPRS on a standard vehicle, the vehicle body does not allow the possibility of installing the power unit outside. Another important reason was that structural changes to the truck must

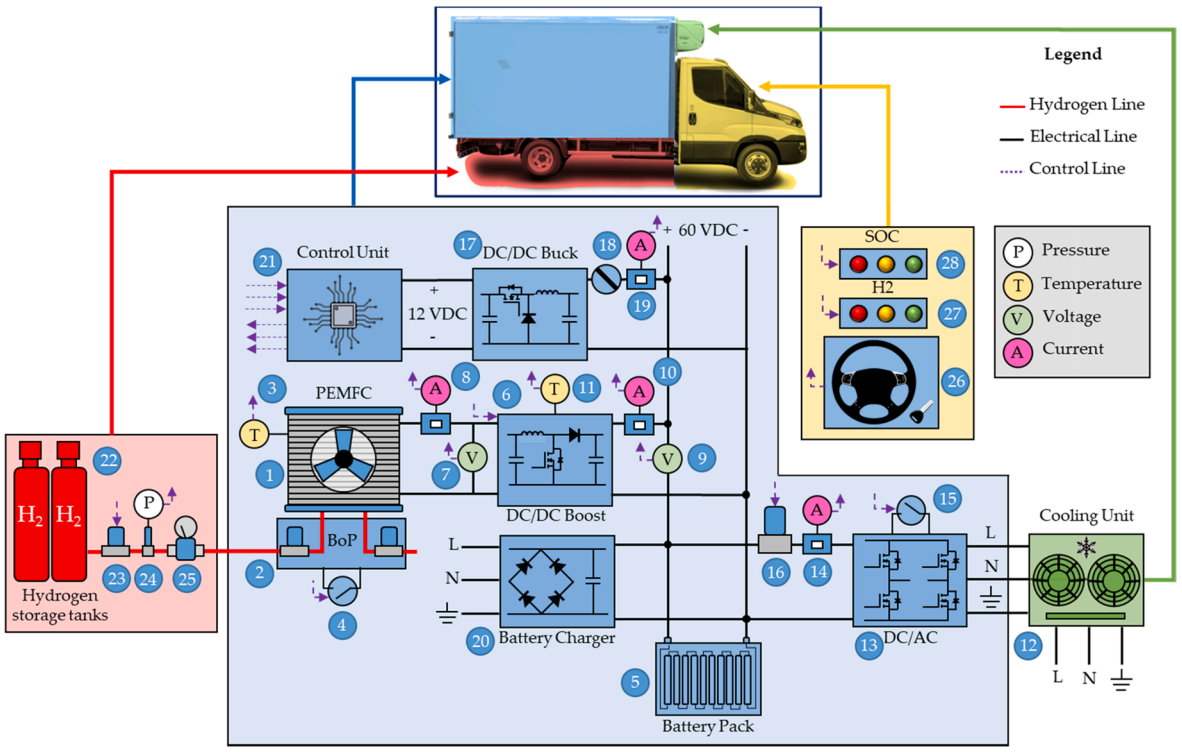

Fig. 4. Hydrogen-powered refrigeration system. Component layout.

be kept to a minimum to comply with current regulations. In addition, this location isolates the power unit from the high temperatures caused by the vehicle's exhaust gases. To prevent the heat generated by the PEMFC and the power equipment from accumulating in the enclosure, a forced air inlet and outlet to the outside has been provided in the refrigerated box of the vehicle. These ducts have been duly protected to avoid thermal bridges and the entry of rain from the outside.

The hydrogen storage system was located on the sides of the truck (red zone, Fig. 4), just below the refrigerated box, for manoeuvrability and safety reasons. Thus, the chosen location allows easy access to the pressurized hydrogen bottles, so that they can be replaced quickly and safely. In addition, this location prevents the formation of explosive atmospheres in the event of a hydrogen leak.

Finally, the general control was integrated into the vehicle cabin, right next to the driver's seat. (Yellow area, Fig. 4).

In the following, each of the three systems will be analysed and described.

First, considering the power unit, it is based on a commercial 2 kW PEMFC (1, Fig. 4), which also integrates its BoP and local control (2, Fig. 4). It manages the supply and purge solenoid valves, the thermal control of the stack (it incorporates a temperature sensor that manages the axial fans to cool and oxygenate the stack) and the electrical connection to the load. For operation, an external 12 VDC power supply is required. In addition, to implement the developed control law (Section 2.3.3), an additional thermoresistance-type ambient temperature sensor has been installed (3, Fig. 4). Finally, a control relay (4, Fig. 4) has been incorporated into the BoP management system which, commanded by the control unit (21, Fig. 4), allows the PEMFC to be switched on or off remotely.

According to the operation already described, the PEMFC is used to charge the battery (5, Fig. 4). For this purpose, the developed DC/DC boost converter ensures the correct integration and operation of the PEMFC on the DC bus (6, Fig. 4).

To implement the PEMFC power management algorithm, the DC/DC boost converter integrates voltage and current sensors (7 and 8 respectively, Fig. 4) at its input to measure the PEMFC operating variables. Similarly, to measure the DC bus voltage and the power delivered by the PMEFC + DC/DC converter assembly, voltage and current sensors are integrated at its output (9 and 10 respectively, Fig. 4). Finally, for thermal management of the DC/DC boost converter, two axial fans with ON/OFF control are installed. They are activated by the thermoresistance-type temperature sensor (11, Fig. 4) mounted on the power heatsink. If for any reason the temperature remains abnormally high despite ventilation, the control unit will shut down the converter.

The battery powers the cooling unit (12, Fig. 4) through a DC/AC converter (13, Fig. 4) when the vehicle is stopped or parked (contact off, 26 Fig. 4). The AC operation allows power supply from the electricity grid or from the developed HPRS (Fig. 1), in both cases single-phase 230 VAC. DC/AC converters are available on the market for the required ratio, so a commercial DC/AC converter was chosen, specifically the model Mars Rock 8,000 W by CNBOU®. The DC/AC consumption from the DC bus is monitored by a current sensor (14, Fig. 4). For remote control, the DC/AC converter incorporates a control relay (15, Fig. 4), whose closing or opening determines its connection or disconnection and, therefore, the power supply to the refrigeration unit. Finally, for safety reasons, a high-current DC contactor (16, Fig. 4) is located between the battery and the single-phase DC/AC converter to ensure electrical isolation when required. This contactor is open when the vehicle is running or during maintenance work.

A DC/DC buck converter (60 to 12 VDC) is required to power all the HPRS auxiliary electronics from the DC bus. The Delta Electronics® model B62SR12424AC was chosen for this purpose (17, Fig. 4). The power consumption of all the auxiliary electronics is monitored by a current sensor (19, Fig. 4). A main switch (18, Fig. 4) that can be manually operated by the driver allows the HPRS to be turned on or off at the beginning or end of the working day, respectively.

To ensure the operation of the HPRS in all circumstances, and to make it as versatile as possible, an auxiliary battery charger has been included (20, Fig. 4). This device allows the battery to be charged from the electricity grid (Fig. 1) when hydrogen is not available or there is a problem with the PEMFC.

Finally, the monitoring of the sensors and the control of all the

actuators and, in general, of the entire HPRS, is performed by a centralised control unit specifically designed for this application based on an ATmega2560 microcontroller (21, Fig. 4).

The hydrogen storage system (red zone, Fig. 4), located on the sides of the vehicle, consists of two Carbotainer® B20 bottles (22, Fig. 4). Each bottle has a capacity of 20 L and stores compressed hydrogen at 200 bar. Hydrogen is supplied through a pipeline incorporating a solenoid valve (23, Fig. 4) to control the opening/closing of the hydrogen flow, and a pressure sensor (24, Figure) to estimate the volume of hydrogen stored in the bottles from the pressure measurement. It also incorporates a two-stage regulator to adapt the 200 bar pressure of the hydrogen bottles to the 0.5 bar pressure of the supply line to the PEMFC (25, Fig. 4).

Finally, the elements located in the vehicle cabin (yellow area, Fig. 4) will be considered. First, there is a vehicle start detection circuit (26, Fig. 4). This circuit provides the control unit with an ON/OFF signal to detect the ignition key. It is important to remember that the activation or deactivation of the vehicle's ignition key will determine whether the developed HPRS will be turned on or off. Regarding the interface with the vehicle driver, an indicator panel with LEDs is also incorporated to show the HPRS status. The first part of the panel consists of three LEDs indicating the hydrogen level in the bottles (27, Fig. 4): high (green), medium (orange) or low (red). The second part of the panel consists of three LEDs indicating the state of charge (SOC) of the battery (28, Fig. 4): high (green), medium (orange) and low (red).

Table 2 summarizes the main technical characteristics of all the elements that, after a careful survey of the market, have been selected for the HPRS, including the model and the manufacturer.

Table 2
Main technical characteristics of the hydrogen-powered refrigeration system.

Components			
Component	Model	Manufacturer	Main characteristics
PEMFC	2000 W air-cooled	Horizon®	Type of fuel cell: PEM Number of cells: 48 Rated Power: 2000 W Performance: 28.8 V @ 70 A Max stack temperature: 65 °C H2 Pressure: 0.45–0.55 bar. Efficiency of stack: 40% @ 28.8 V
Hydrogen bottles (x2)	B20	Carbotainer®	Capacity: 20 l (40 l total) Maximum stored hydrogen: 3.5 Nm^3 (7 Nm^3 total) Operating pressure: 200 bar Ø 265 mm × length 823 mm
Battery	Samsung 50E	Samsung®	Nominal voltage: 60 VCapacity: 120 Ah (7.20 kWh)
DC/AC converter	Mars Rock 8000 W	CNBOU®	Rated power: 8000 W (16000 W peak power) Frequency: 50 Hz / 60 Hz
DC/DC buck converter	B62SR12424AC	Delta Electronics®	Input voltage range: 18 ~ 106 V 200 W Output @ 18 V ~ 27 V Vin range
DC/DC boost converter	Interleaved architecture	Developed by authors	Input voltage range: 20 ~ 50 V 2000 W Output @ 40 V ~ 100 V Vin range

2.3. Energy management system

2.3.1. Control logic of the hydrogen-powered refrigeration system

To increase the performance and lifespan of the HPRS, operating priorities are set on a device-by-device basis. Thus, the battery always guarantees the electrical demand of the electric compressor, while the PEMFC will act as a range extender. In other words, the PEMFC will be used to charge the battery, maintaining its operation at constant power (rated power), regardless of whether the refrigerated vehicle is stationary or in motion. This premise has a dual purpose: to avoid successive start/stop cycles and abrupt changes in the PEMFC power profile, which could lead to a reduction in its lifespan [33,34]. Operating the PEMFC at rated power aims to increase system performance and minimize battery charging time, so that the HPRS responds even to the most unfavourable load profiles, corresponding to routes with a high frequency of stops.

Considering the above, the EMS of the HPRS is described as follow, Fig. 5 and Fig. 6. The EMS implements two parallel controls, one for the battery and other for the PEMFC. These controls will depend on the battery voltage and the ignition key, however, the PEMFC can charge the battery regardless of whether the ignition key is on or off. Assume that the battery is initially charged and that, while the VPE is running (ignition key on), the RS makes use of the VPE and its internal battery to drive the mechanical compressor. At this point, the HPRS remains in standby mode (Fig. 6), which is characterised by the disconnection of the PEMFC and the electrical isolation of the battery and the DC/AC converter.

When the driver stops the VPE (ignition key off), the HPRS stats working (Fig. 6). At this moment, the EMS evaluates the battery voltage (V_{Bat} that is equal to $V_{DC_{Bus}}$) and, if its value is higher than the preset minimum safety value ($V_{Bat_{min}} = 50$ VDC, 3.125 VDC/cell, or $SOC = 20$ % approximately), Fig. 6, it activates the DC contactor, allowing the battery to power the electric compressor through the DC/AC power converter. Consequently, the battery supplies the power to the RS. This will cause a prolonged discharge of the battery until its voltage reaches the preset minimum value ($V_{Bat_{FC}} = 54.4$ VDC, 3.4 VDC/cell), Figs. 5 and 6. Then, the EMS evaluates the level of hydrogen stored in the bottles (H_2) and the temperature of the DC/DC power converter (T_{DCDC}). If the hydrogen level is higher than the minimum ($H_{2_{min}} = 10$ bar, equivalent to 400 L (5 %) of maximum stored hydrogen) and the temperature is lower than the maximum value ($T_{DCDC_{max}} = 65$ °C), it will activate the hydrogen supply line and the PEMFC (Fig. 6). Subsequently, the DC/DC boost power converter is activated, and the PEMFC is started in a controlled manner using a step-up profile until the rated power of the PEMFC is reached, Fig. 6. This procedure is intended to reduce the thermal and electrical stress during the PEMFC start-up interval. The $H_{2_{min}}$ value corresponds to the minimum volume of hydrogen that ensures a controlled shutdown of the PEMFC and a minimum hydrogen pressure enough for the two-stage regulator to function properly (25, Fig. 4). The $T_{DCDC_{max}}$ has been selected to ensure a maximum safety temperature of the power semiconductors of approximately 80 °C, considerably lower than their maximum allowable temperature, 120 °C.

When the PEMFC reaches its rated power, its controller keeps it running until one of the shutdown conditions occurs: maximum battery voltage ($V_{Bat_{max}} = 64$ VDC, 4 VDC/cell), low hydrogen level ($H_{2_{min}}$), high operating temperature of the DC/DC boost power converter ($T_{DCDC_{max}}$) or high ambient temperature, Fig. 6. Remember that the HPRS is in an isothermal enclosure (see Fig. 4), so it is necessary to control the ambient temperature. The first three conditions are mandatory and, therefore, determine the immediate shutdown of the PEMFC, while the high ambient temperature situation is a less restrictive condition, allowing corrective actions to ensure the continuous operation of the PEMFC. To this end, the control system regulates the operating power of the PEMFC so that its temperature does not reach the maximum safe operating limit, see Section 2.3.2.

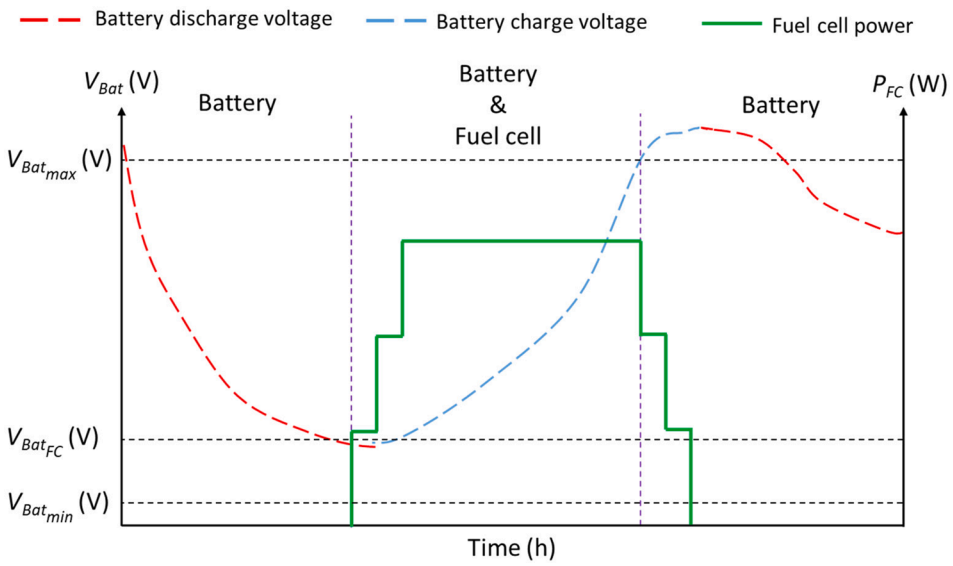

Fig. 5. Hydrogen-powered refrigeration system. Battery/Fuel cell interoperability.

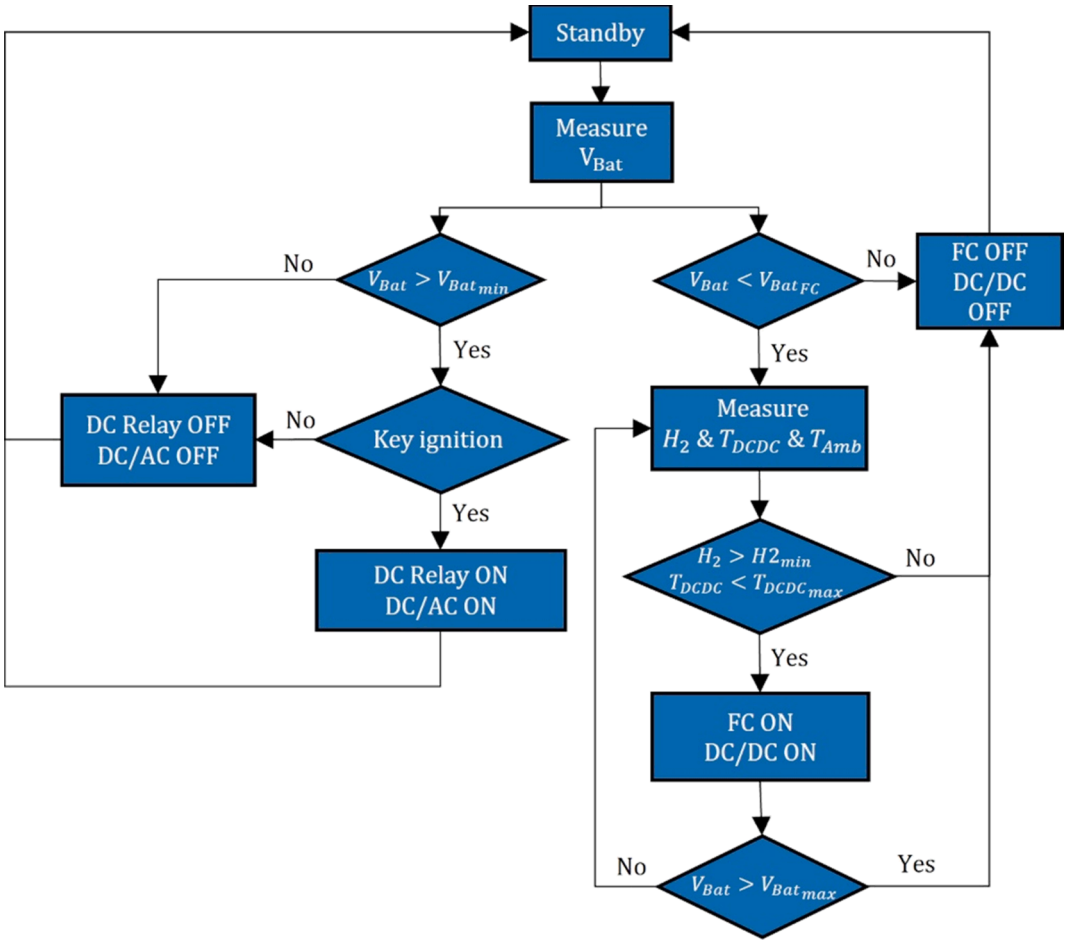

Fig. 6. Hydrogen-powered refrigeration system. Control logic diagram.

Finally, as long as the stored hydrogen level allows, the charging process will continue until the battery voltage reaches the upper limit, $V_{Bat_{max}}$, after which the PEMFC will be shut down in a controlled manner, using a step-down profile, until the PEMFC is completely shut down and the hydrogen supply line is closed, Fig. 5 and Fig. 6.

This described process will be repeated indefinitely during the operation of the RS until all the stored hydrogen is consumed or the working day is over. Table 3 lists the characteristic and limit values that define the operation of the developed HPRS.

Table 3
Characteristic values and operating limits of the hydrogen-powered refrigeration system.

Parameter	Value	Meaning
$V_{Bat\,min}$	50 VDC	Minimum battery operating voltage, equivalent to a SOC = 20% approximately
$V_{Bat\,FC}$	54.4 VDC	Battery voltage causing operation of the PEMFC
$V_{Bat\,max}$	64 VDC	Maximum battery operating voltage
$H_{2_{min}}$	10 bar, 400 L	Minimum hydrogen level calculated in terms of pressure (10 bar) and volume of hydrogen (5% of maximum)
$T_{DCDC_{max}}$	65 °C	Maximum temperature of the heatsink of the interleaved DC/DC boost converter

2.3.2. Control algorithm of the fuel cell and DC/DC converter

A modified perturbation and observation (P&OM) algorithm were developed to determine the operating power of the PEMFC regardless of the operating humidity, temperature or accumulated degradation. This algorithm aims to ensure maximum power transfer of the PEMFC (remember that the PEMFC has a variable load at its output) throughout its lifespan, providing excellent results without the need for a mathematical model that captures the dynamic, thermal behaviour and degradation rate of the PEMFC.

The developed P&OM algorithm is based on the classical P&O, widely used in photovoltaic systems [35,36]. In this case, the obtaining of the maximum power point (MPP) is based exclusively on the experimental behaviour of the PEMFC polarization curve. Specifically, on the relationship between the slopes of the voltage-current (V – I) and power-current (P – I) curves. Thus, according to Fig. 7, the MPP is determined as the point on the polarization curve at which the derivative of the power with respect to the PEMFC voltage is zero ($\frac{\Delta P_{FC}}{\Delta V_{FC}} = 0$). Similarly, the slope of the V-I and P-I curves will determine the corrective actions to localize the MPP against disturbances in the polarization curve due to variations in the instantaneous operating conditions, thereby increasing or decreasing the operating voltage of the PEMFC, depending on whether it operates in the region defined by $\frac{\Delta P_{FC}}{\Delta V_{FC}} < 0$ or $\frac{\Delta P_{FC}}{\Delta V_{FC}} > 0$ respectively.

On the other hand, modifications to the classical P&O algorithm guarantee two fundamental conditions to preserve the safe and constant operation of the PEMFC: the adequacy of the power limit to thermal stress and the non-operation at low voltage values.

As mentioned above, a high outdoor ambient temperature or a failure of the forced ventilation circuit can cause a controlled shutdown of the PEMFC due to thermal stress, which would interrupt the power supply to the DC bus. Since it is not possible to act on the BoP, being a commercial system and therefore closed, to ensure continuity of power supply in any circumstance, a modification of the classic P&O algorithm is established. This modification in the control law is based on the imposition of a maximum permissible operating power, $P_{FC_{SP}}$, as a function of the ambient temperature (T_{amb}), thus posing a tracking problem with respect to the operating power of the PEMFC (P_{FC}), Fig. 7.

The $P_{FC_{SP}}$ calculation is based on the mathematical model (17), obtained from the experimental characterization of the PEMFC operating temperature (T_{FC}) for different power values, considering the ambient temperature inside the enclosure and for the most unfavourable case, i.e., without forced ventilation, see Fig. 8a. Measurements were performed once the stable operating temperature regime was reached.

From this characterization, it is possible to determine the thermal gradient (ΔT_{FC}) associated with each operating power of the PEMFC, Fig. 8a. With its value, and for a given value of ambient temperature, it is possible to determine the maximum operating power that ensures that the temperature of the PEMFC does not exceed the safe operating limit (65 °C). In this case, the power setpoint is correctly set to a linear function with respect to the ambient temperature, Fig. 8c.

$$P_{FC_{SP}} = -48.969 \bullet T_{amb} + 3662.2 \tag{17}$$

Finally, to ensure an efficient and conservative use of the PEMFC, a lower operating voltage limit is set to allow the PEMFC to operate within its standard operating range, defined by the activation and ohmic regions. In this way, a high operational performance is ensured, avoiding working in the concentration region, which could lead to a higher degradation rate associated with the occurrence of hot spots or gas starvation phenomena [37,38]. Then, if the operating voltage is lower than the limit value, the control law establishes a tracking problem with respect to the preset voltage limit ($V_{FC_{SP}} = 25$V), see Figure.

Considering the operating principles of the described P&OM algorithm, Fig. 9 describes the control logic implemented in the local control of the DC/DC boost converter to manage the operating power of the PEMFC. Its operation is described below.

It is an iterative procedure and starts from the measurements of the PEMFC current and voltage variables, as well as the ambient temperature in the enclosure. From them, the value of the current operating power of the PEMFC is obtained, as well as, from equation (17), the

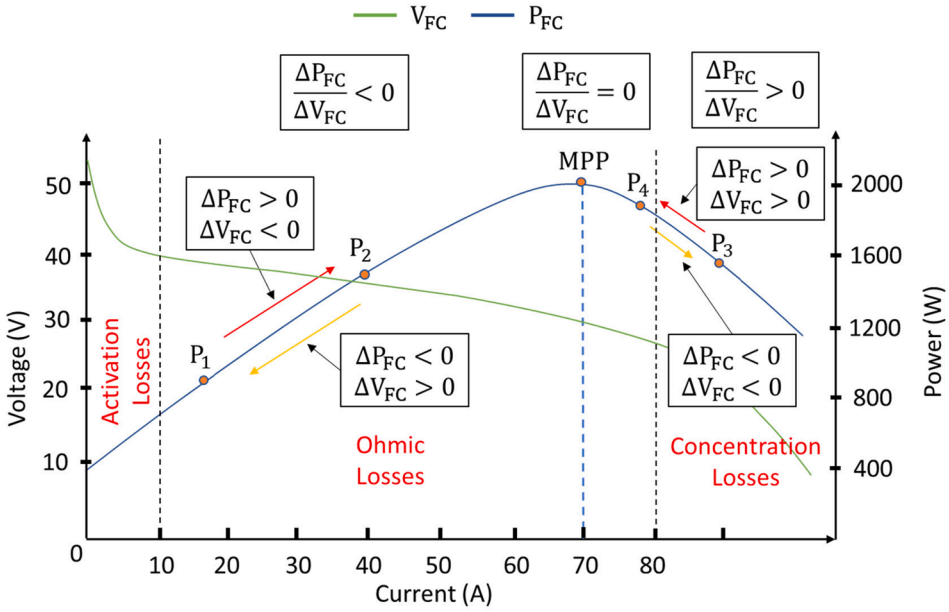

Fig. 7. Working principle of the modified perturbation and observation algorithm.

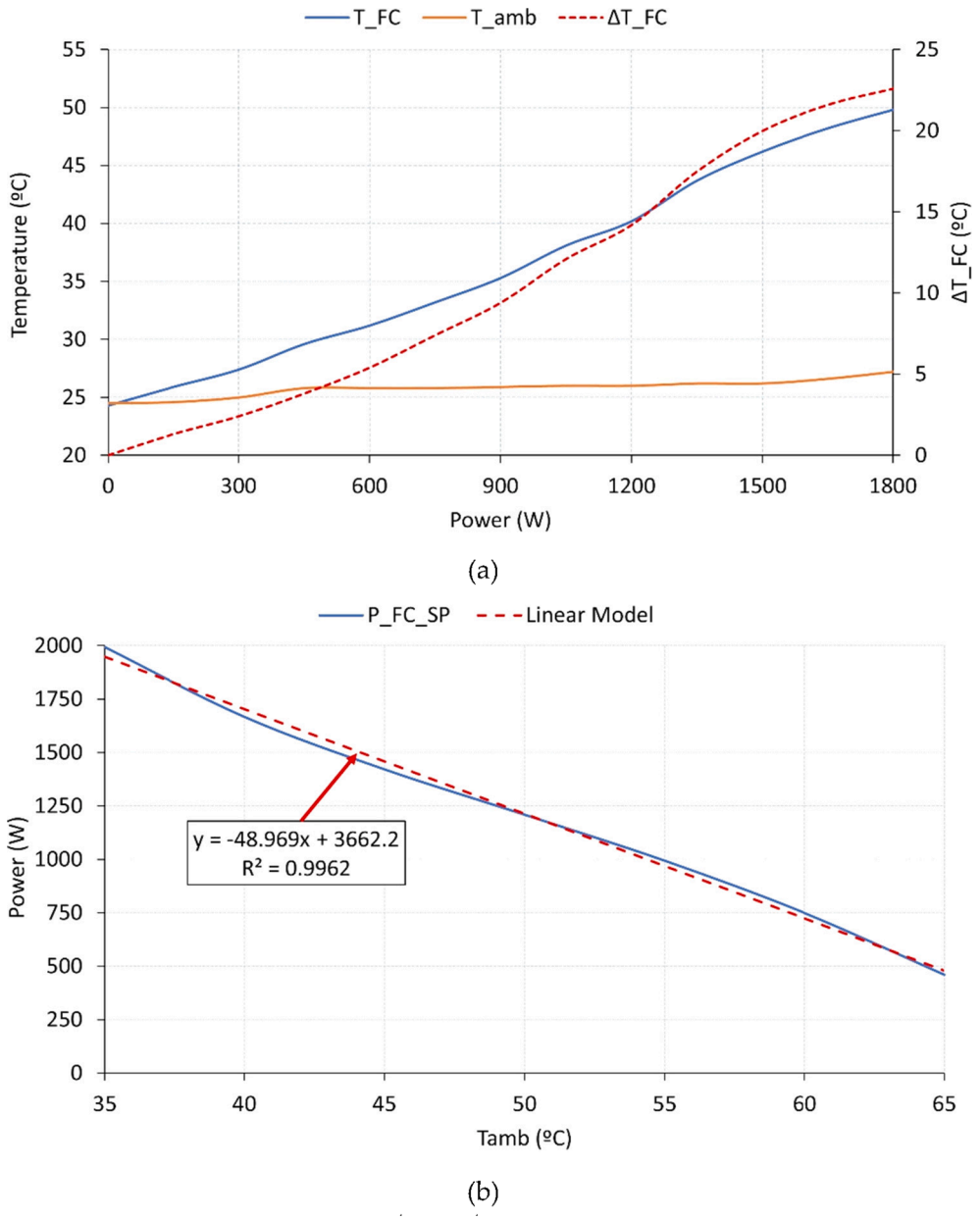

Fig. 8. PEMFC behaviour. (a) PEMFC operating temperature with respect to operating power and ambient temperature and PEMFC temperature variation; (b) Maximum PEMFC power and polynomial model with respect to ambient temperature.

power set-point according to the thermal criterion. Then, following the flow of the developed P&OM algorithm, the slope of the curve defined by the PEMFC power and voltage is evaluated to locate the MPP. Thus, as depicted in Fig. 7, a slope $\frac{\Delta P_{FC}}{\Delta V_{FC}} > 0$ indicates the need to increase the PEMFC operating voltage to shift the operating point to the left, i.e., it is necessary to reduce the PEMFC operating current, and therefore, the demand on its terminals. For this purpose, the local controller of the power converter will decrease its δ in jumps ($\Delta\delta$) set at 0.5%. Remember that δ can vary from 1 to 0, so 5% is 0.05.

Conversely, if the slope $\frac{\Delta P_{FC}}{\Delta V_{FC}} < 0$, it indicates the need to reduce the operating voltage of the PEMFC, to shift the operating point to the right. This requires increasing the PEMFC operating current and, therefore, the demand on its terminals. Now, unlike the previous case, the local controller of the power converter will increase its δ by $\Delta\delta = 0.5$ %. This operation can be performed if, and only if, the power and operating voltage of the PEMFC are within the limits set by the thermal stress and minimum voltage constraints described above. Thus, if the PEMFC power is higher than that defined by $P_{FC_{SP}}$, or the operating voltage is lower than $V_{FC_{SP}}$, the local controller of the DC/DC boost converter will proceed to reduce δ to prioritize thermal stress and degradation criteria over the maximization of the operating power.

Based on the design assumptions of the developed P&OM algorithm, the proposed control structure for the PEMFC and interleaved DC/DC boost converter assembly is schematically presented in Fig. 10.

3. Implementation and Experimental Results

In this section, the experimental validation of the HPRS and the EMS developed and described in section 2.3 is carried out. For this purpose, an experimental validation was carried out on a commercial vehicle, specifically, a Mercedes-Benz® Sprinter 311 CDI light refrigerated truck, Fig. 11a. It was equipped with the Thermo King® V-200 electric refrigeration system shown in Fig. 11b, and with the isothermal refrigerated box shown in Fig. 11c. Fig. 11 shows the vehicle as it came from

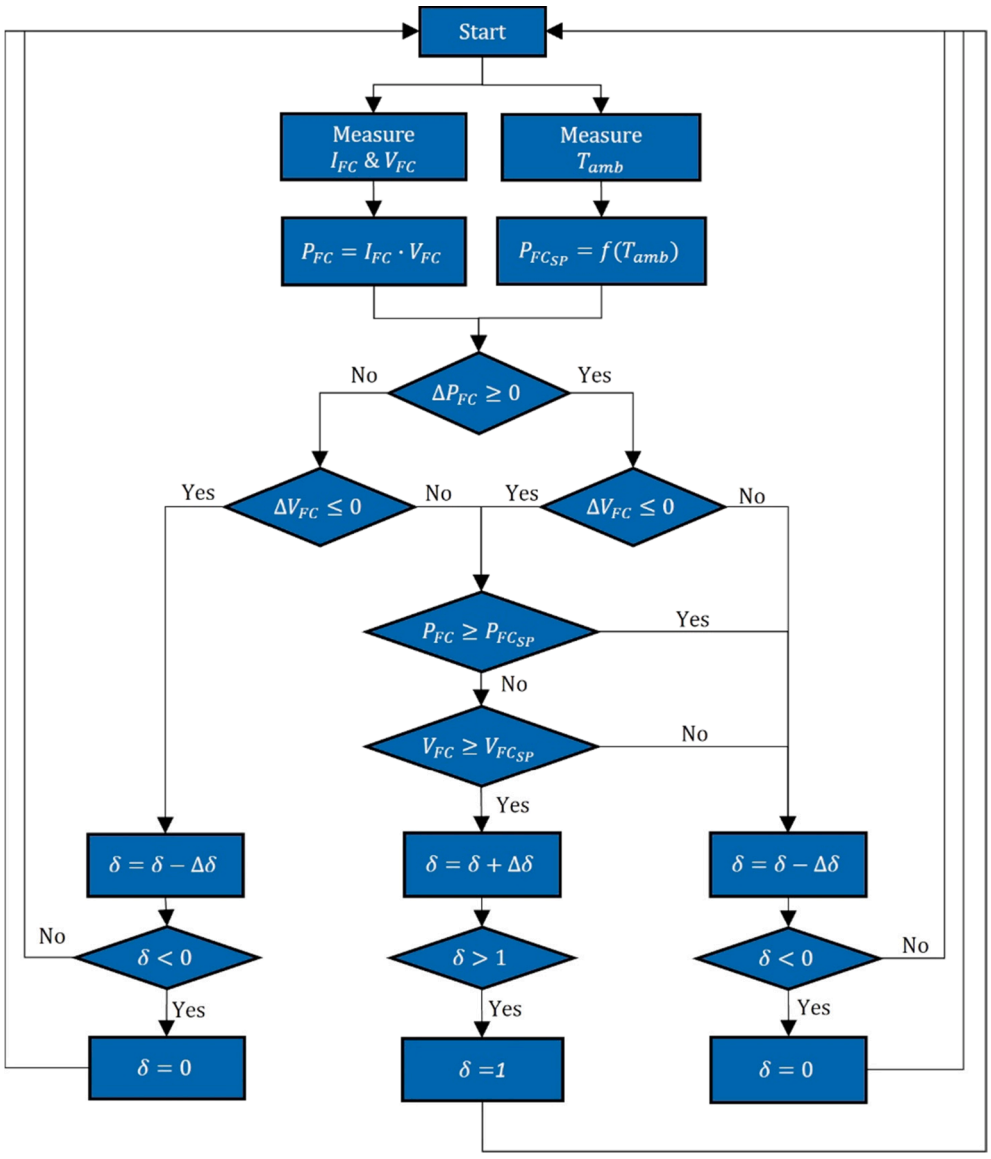

Fig. 9. P&OM algorithm developed *to track the MPP of the PEMFC.*

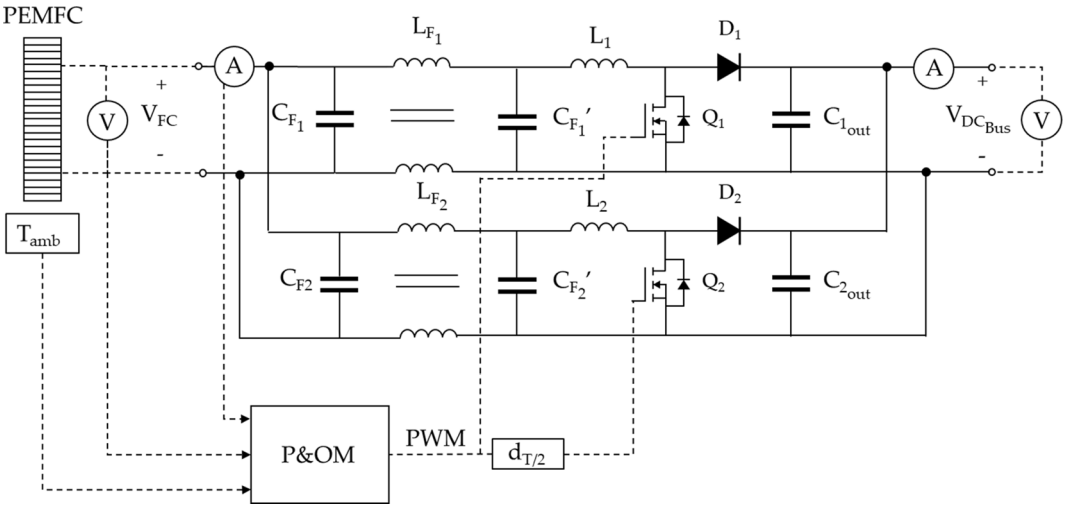

Fig. 10. Schematic diagram of PEMFC and DC/DC converter assembly with P&OM.

Fig. 11. (a) Detail of the light refrigerated truck; (b) electric refrigeration system; (c) isothermal cool box.

the factory, just purchased.

On the other hand, Fig. 12 shows the final assembly of the developed HPRS on the vehicle. Fig. 12a shows all the elements inside the isothermal box manufactured for this purpose, housed in the vehicle's refrigeration box (note the detail of the external ventilation duct). Fig. 12b shows the detail of part of the developed electronics, specifically the control unit and the interleaved DC/DC boost converter. Finally, Fig. 12c shows the hydrogen storage system located on the vehicle frame in a specially designed metal box, according to the location described in section 2.2 and shown in Fig. 4.

The experimental test consisted of subjecting the vehicle to a normal working day, in accordance with the characteristics set out in the first paragraph of section II, where the design conditions are established. Since the vehicle was not yet approved for use on public roads and urban areas, the experimentation was conducted on a circuit closed to traffic of approximately 2.5 km in length, covering a university campus and its surroundings, Fig. 13.

The duration of the test was the equivalent of one working day, 8 h, starting at 7:00 am and ending at 15:00 pm. The vehicle was loaded with fruit and the set point temperature of the RS was set at 4 °C. During the test, travel times at controlled speed (urban, <50 km/h), vehicle stops, parking for unloading the goods and isothermal box door opening times were carried out, always following the indications provided by a company specialized in this type of transport. Throughout the working day, the HRPS operating profile was as shown in Fig. 14. This Figure is to be interpreted as follows: when the vehicle is in motion, the HPRS is off (state = 0) and the compressor of the refrigeration system (the mechanical one in this case, see Fig. 1) is powered by the VPE. When the vehicle stops and its engine shuts down, the HPRS is activated (state = 1), powering the compressor of the refrigeration system (the electrical one in this case, see Fig. 1).

The initial conditions were set at the usual working values: 80% of the battery SOC and 6 m^3 of stored hydrogen, corresponding to 85% of the maximum hydrogen capacity.

The results obtained in the experimental test are shown in Figs. 15-19. Specifically, Fig. 15 shows the power supplied/consumed of the elements that compose the HPRS: PEMFC + DC/DC boost converter, battery, DC/AC converter and auxiliary consumptions for the entire experimental test. Remember that the DC/AC power corresponds to the power of the electric compressor, considering its corresponding efficiency. Null values of DC/AC converter power correspond to periods of the vehicle in motion since the RS is supported by the mechanical compressor. Non-zero values correspond to the power consumption of the RS, supported by the electric compressor when the vehicle is stopped for food delivery. The sign criteria are as follow: current and power variables will be considered positive if they are injected to the DC bus, while current or power variables will be considered negative if they are extracted from the DC bus.

Fig. 16 shows the electrical variables of the battery, i.e., the DC bus voltage together with the characteristic and limits values defined in Table 3, as well as its charging/discharging current.

Fig. 17 shows the time evolution of the battery SOC, and the level of hydrogen stored in the bottles during the experimental test.

Finally, Figs. 18 and 19 show the main operating variables of the PEMFC, i.e., voltage, current and power, as well as the value of the voltage and power set points as function of the ambient temperature inside the isothermal enclosure, according to the P&OM algorithm defined in section 2.3.

4. Discussion

As an initial premise for understanding the control strategy developed, it has been considered that the PEMFC must guarantee the correct SOC of the battery, which is controlled by its terminal voltage. Thus, as defined in the control logic developed and presented in Figs. 5 and 6, the PEMFC start-up criterion is set as a function of the voltage at the terminals of the lithium-ion battery pack, not the route time or the energy demanded. The minimum voltage value at which the PEMFC starts to operate ($V_{Bat_{FC}}$) has been selected considering the SOC and the minimum operating voltage ranges to ensure the correct power supply to the refrigeration unit while the PEMFC start-up protocol takes place. Thus, when the battery voltage, due to the progressive discharge, reaches the predefined value of 54.4 VDC, the EMS performs the controlled start-up of the PEMFC, see Figs. 15 to 19 (t = 190 min).

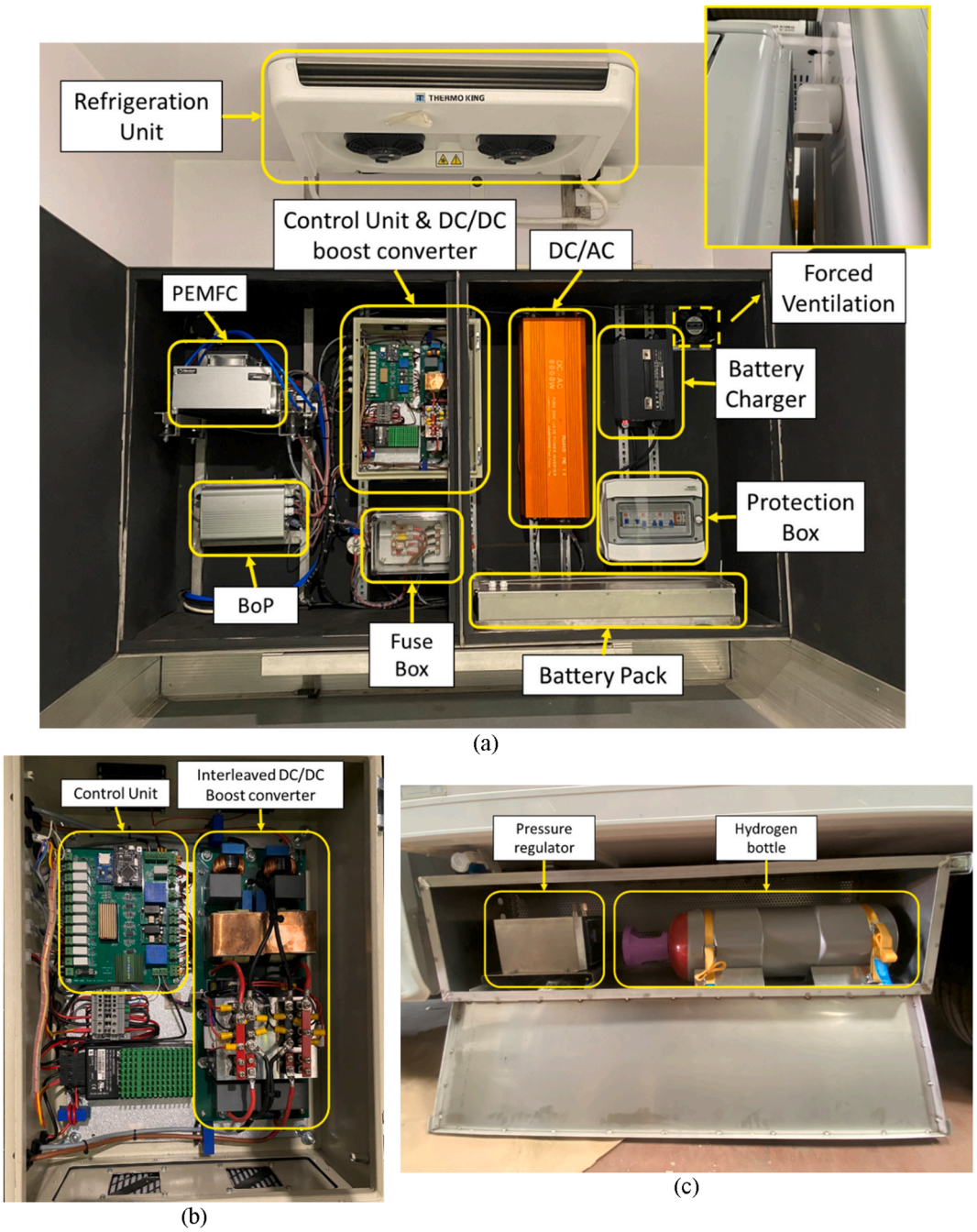

Fig. 12. Distribution and final assembly of the developed hydrogen-powered refrigeration system on the vehicle. (a) Detail of the control unit and the interleaved DC/DC boost converter. (c) hydrogen bottle, pressure regulator and security pipeline.

Another important aspect to take into account before discussing the results is that, since the objective of the research is to demonstrate the technical and economic feasibility of the proposal through a real application example, for the sizing criteria of the HPRS, the authors have relied on their experience in other similar projects, where a compromised solution that guarantees a correct operation is a homogeneous distribution in terms of energy between the battery pack and the hydrogen system. Thus, for the sizing of the battery pack and the hydrogen system, an approximate energy split of 50% has been considered. Of course, it is assumed and understood that, although it works very well, this is an empirical decision. It would be interesting to face in future works, with detailed knowledge of the trajectory and the driving and stopping times for a given application, to apply optimisation techniques to solve the multi-objective sizing problem that guarantees the lowest cost of the HPRS with the greatest autonomy.

Considering the results obtained, Fig. 15 represents the RS operation of the vehicle during an 8 h working day (480 min). While the VPE is running, the mechanical compressor ensures the RS operation, but when the vehicle stops, the RS is powered by the electric compressor through the DC/AC converter. Therefore, the P_{DCAC} shows the demand profile of the electric compressor and, ultimately, the profile to be ensured by the HPRS. Based on the above, adding up all the time the electric compressor is on (state = 1 in Fig. 14, and $P_{DCAC} \neq 0$ in Fig. 15), it is observed that practically half of the time the vehicle is stopped for varying time intervals, corresponding to stops for food delivery, specifically 4.2 h, compared to 3.8 h when the vehicle is in motion.

Initially, the DC bus voltage is $V_{DC_{Bus}} > V_{Bat_{min}} = 50$ VDC, Fig. 16, and the battery SOC is high (greater than80%, Fig. 17), so the battery

Fig. 13. Circuit closed to traffic used for the experimental test.

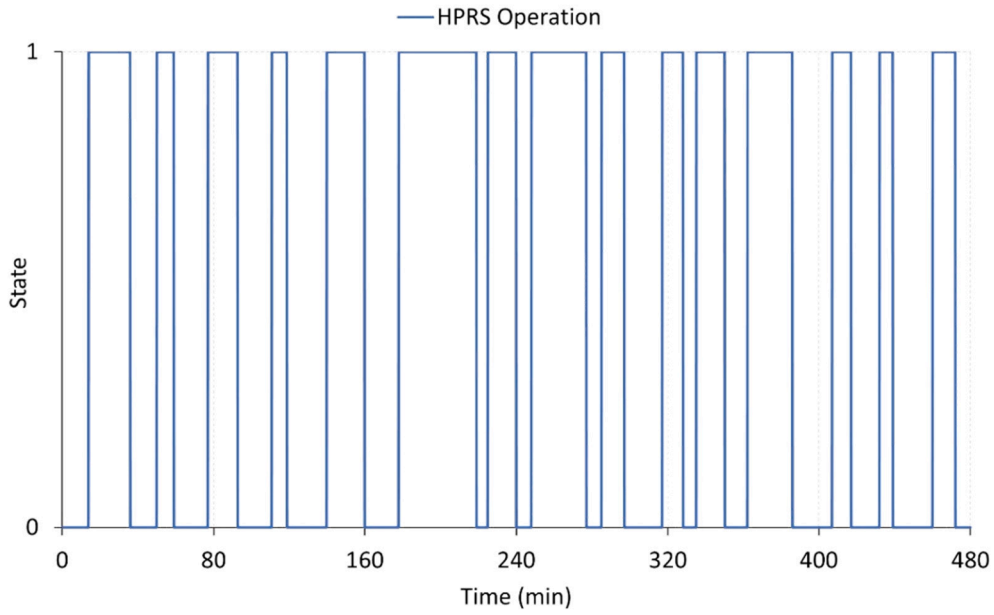

Fig. 14. Operating states of the HPRS system during the experimental test.

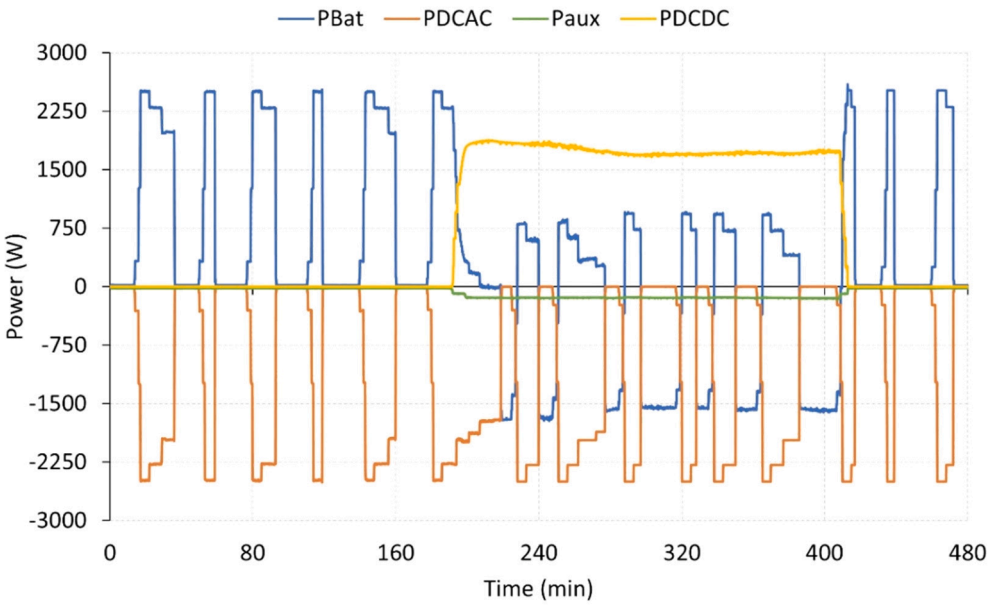

Fig. 15. Battery power (PBat), DC/AC converter power (PDCAC), auxiliary equipment power (Paux) and boost DC/DC converter power (PDCDC) during the experimental test.

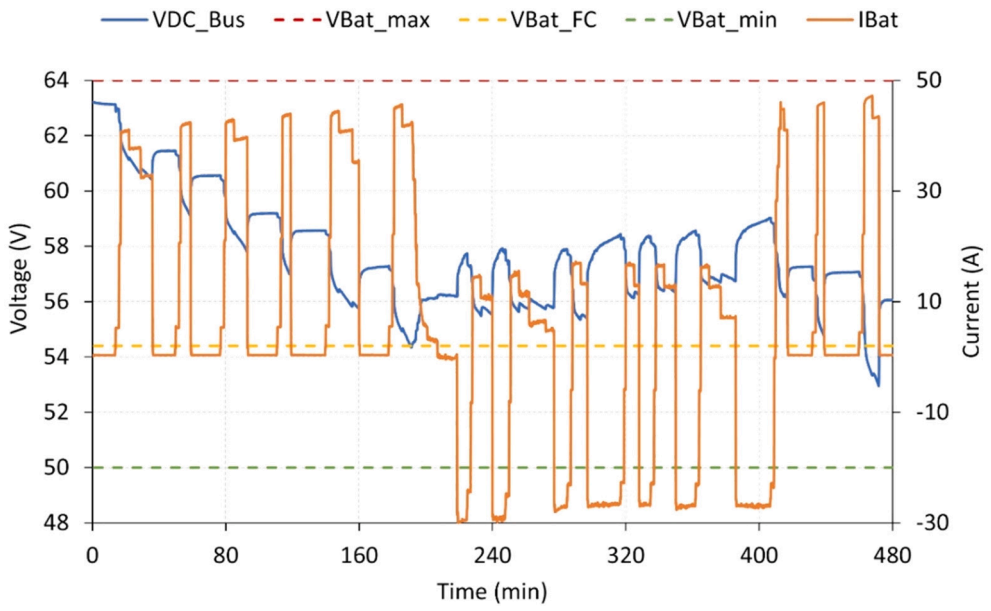

Fig. 16. DC Bus voltage and battery current during experimental test.

supplies the power demanded by the electric compressor, Fig. 15. Consequently, this causes the battery to discharge, which is reflected in the evolution of the DC bus voltage and the SOC level, until the preset safety value is reached, $V_{DC_{Bus}} = V_{Bat_{FC}} = 54.4\ VDC$, $t = 190$ min, Figs. 16 and 17 respectively. This determines the start-up of the PEMFC, according to the control logic and diagram described in section 2.3.1 and Fig. 6 respectively. During this stage, the consumption of the auxiliary equipment is very low, and is associated with the power consumption required to ensure the operation of the control and power electronics, $P_{aux} < 15$ W, Fig. 15.

To start up the PEMFC, the hydrogen volume available in the bottles is estimated by measuring the pressure, obtaining a value of approximately 6,000 L (85% of the maximum volume), much higher than the minimum established, Fig. 17, so the PEMFC activation protocol is established. This protocol is characterised by a controlled start-up of the PEMFC by imposing a staircase-type rising power profile, with 500 W increments and 2 min long, Fig. 18. This profile seeks to reduce thermal, water and electrical stress due to sudden changes in the operating power of the PEMFC. Similarly, the operation of PEMFC requires power supply for its BoP, mainly for its oxidant/cooling system, so there is an increase in the power consumption of the auxiliary equipment to a value close to 300 W, see P_{aux}, Fig. 15. The power required from the DC bus is provided by the PEMFC through the interleaved DC/DC boost power converter, P_{DCDC}.

During PEMFC operation, the control logic recalculates in real time the preset operating point of the PEMFC according to the P&OM algorithm described in section 2.3.2. Thus, in the initial instants, the ambient temperature inside the enclosure is relatively low ($T_{amb} \approx 20$ °C) and, therefore, according to expression (17), the power setpoint ($P_{FC_{SP}}$) is higher than the maximum power of the PEMFC, so it does not establish a

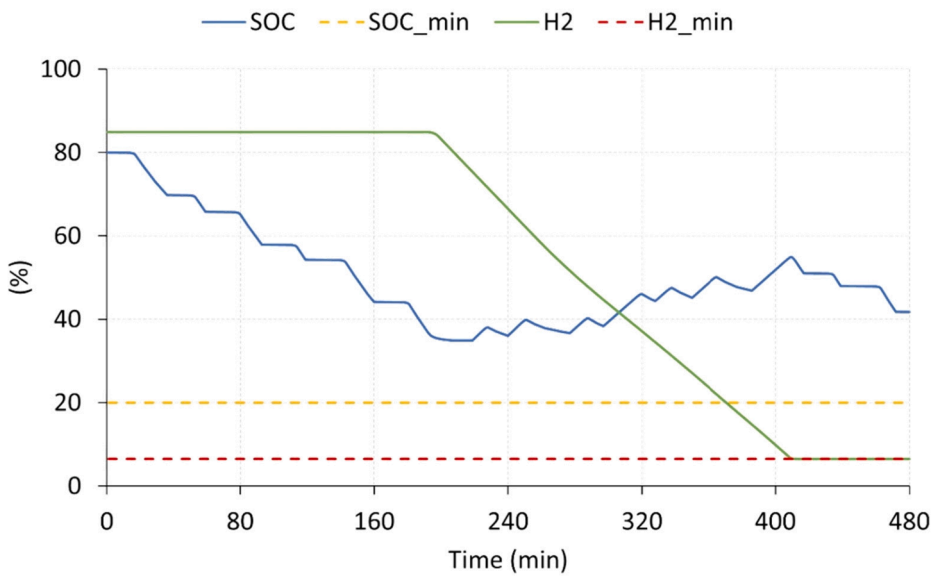

Fig. 17. Battery SOC and Hydrogen level (H2) during experimental test.

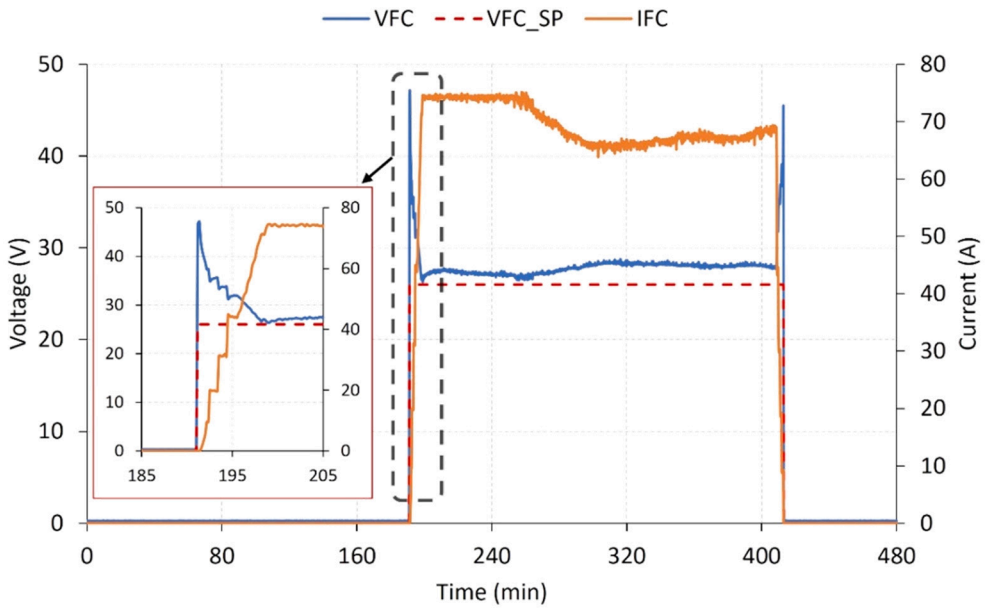

Fig. 18. PEMFC voltage and current profile (VFC and IFC respectively), as well as the voltage set point (VFC_SP) according to the P&OM control law.

limiting condition, Fig. 19. Similarly, the operating voltage of the PEMFC at its MPP is higher than the established minimum voltage, so it also does not establish a limiting condition, Fig. 18. This allows the PEMFC operates at its MPP, maintaining a constant power profile.

As the operation of the PEMFC is prolonged over time, its heat production (efficiency at rated power is around 40%, producing approximately 3,000 W of heat) causes an increase in the internal temperature of the enclosure, see T_{amb}, Fig. 19. This causes the power setpoint of the PEMFC to be reduced to prevent its safety shutdown. Thus, from $t = 240$ min, the power setpoint equals and limits the maximum extractable power of the PEMFC, Fig. 19, to reduce the uncontrolled rise in ambient temperature that would cause its shutdown. The correction of the power setpoint, in accordance with the control law imposed by the P&OM algorithm, achieves the proposed objective and allows stabilizing the ambient temperature at approximately 37 °C, while guaranteeing the operation of the PEMFC, in this case at a power of approximately 1,850 W, Fig. 19. Note that the PEMFC works at nearly constant power, which determines a nearly constant hydrogen consumption rate as well, Fig. 17.

Considering the operation of the developed interleaved DC/DC boost converter, it is demonstrated from Figs. 15, 18 and 19 that it allows the correct integration of the PEMFC into the DC bus, while accurately implementing the developed P&OM algorithm. Finally, from the instantaneous values of PEMFC output power and DC/DC boost converter output power, Figs. 19 and 15 respectively, the instantaneous efficiency of the power converter can be determined, which is approximately 92% $\left(\frac{P_{DCDC}}{P_{FC}} = \frac{1702W}{1850W}\right)$.

Now, considering the power balance, during vehicle stopping, the power demand of the electric compressor is supplied by both the PEMFC and the battery, Fig. 15. Thus, as the demand profile is higher than the power generated by the PEMFC, the battery is discharged to ensure the power balance on the DC bus, $P_{DCAC} + P_{aux} = P_{Bat} + P_{DCDC}$. Therefore, the PEMFC acts as a range extender. On the other hand, when the vehicle

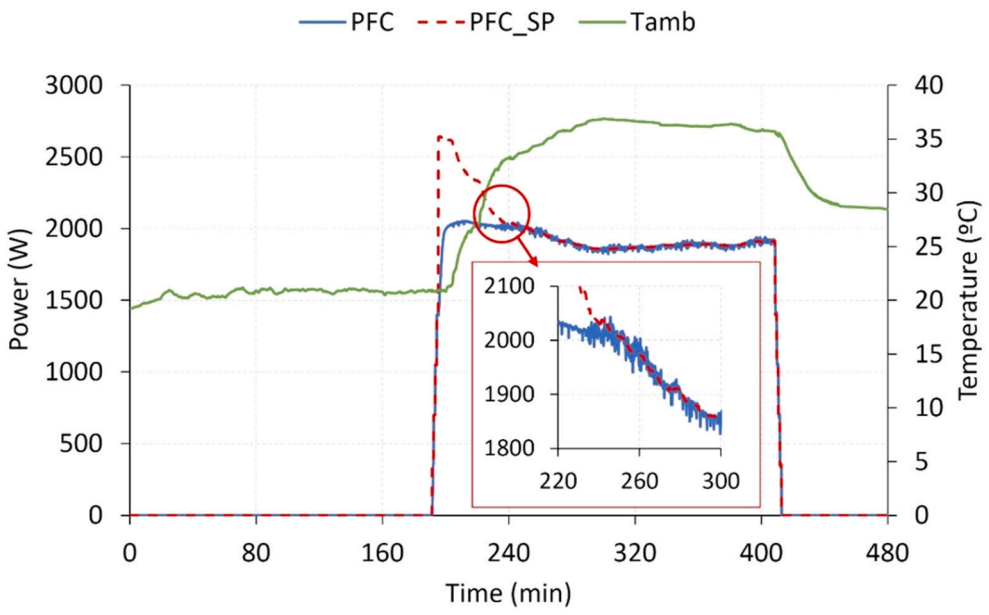

Fig. 19. PEMFC power profile (PFC) and power set point (PFC_SP) according to the P&OM control law and the ambient temperature in the environment of the PEMFC (Tamb).

is in motion, all the energy produced by the PEMFC is fully used to charge the battery, Fig. 15. This is clearly reflected in the DC bus voltage profile and the battery SOC, Figs. 16 and 17 respectively.

According to the EMS developed in Section 2.3, the operation of the PEMFC is maintained over time if the hydrogen level is higher than the minimum set, the DC bus voltage is lower than the maximum preset value ($V_{DC_{Bus}} < V_{Bat_{max}} = 64$VDC) and the DC/DC boost converter is operating below its maximum temperature. In this case, the PEMFC was kept operational for approximately 220 min, until $t = 410$ min, Figs. 15, 18 and 19. At that time, the minimum preset value of the volume of hydrogen stored in the bottles was reached, set at 400 L, which corresponds to a pressure of 10 bars (a hydrogen volume of approximately 5% with respect to the maximum capacity), Fig. 17. This value is sufficient to perform the controlled shutdown protocol of the PEMFC. This protocol is defined by the use of a staircase-type descending power profile, with 500 W steps and 2 min long, Fig. 18. As at start-up procedure, this profile reduces the thermal stress on the PEMFC in the event of a sudden variation in its operating power, especially when the temperature of the PEMFC is high, allowing the BoP's cooling system to progressively cool the PEMFC. After shutting down the converter, the PEMFC, its BoP and its local controller, the solenoid valve in the supply line at the inlet of the two-stage regulator (23, Fig. 4) is closed, isolating the hydrogen bottles, and thus preventing possible hydrogen leaks inside the enclosure.

From $t = 413$ min (Fig. 15), the vehicle continues with its delivery route, however, as the hydrogen resource is not available, the demand profile is guaranteed by the battery, according to the defined EMS. Thanks to the charging previously performed by the PEMFC, the battery voltage and its SOC is considerably higher than the established minimums, $V_{DC_{Bus}} = 59$ VDC and $SOC = 53\%$ (Figs. 16 and 17), thus allowing its use without any restriction. Therefore, until the last stop at $t = 472$ min, coinciding practically with the end of the working day, it is only the battery that supplies the energy required by the electric compressor, Fig. 15. Logically, this operation results in a progressive discharge of the battery, with the consequent reduction of the DC bus voltage and the SOC to a final value of 56 VDC and 41% respectively, Figs. 16 and 17, both values higher than the preset minimums.

From the experimental results, the correct operation of developed HPRS and EMS is validated. It has been demonstrated that it is possible to guarantee the objective of 4 h of autonomy, operating safely, continuously, and smoothly throughout a full working day in a real environment.

Finally, once the correct operation of the developed HPRS has been verified, the analysis in terms of fuel savings, emissions and economic cost will be carried out considering the use of the developed HPRS.

Thus, for the daily consumption profile (7660 Wh) for a working day of 8 h, with parking periods for food delivery of approximately half of the route (4.2 h parked and 3.8 h in motion in the test performed), considering an average energy input per unit volume of 10.7 kWh/litre of diesel, and a thermal efficiency of the diesel engine of approximately 40%, a fuel saving of approximately 1.8 L per day is estimated. If it is also considering that in the case of the exclusive use of the mechanical compressor, it is necessary to keep the VPE started to ensure the operation of the RS during stops, with an estimated consumption of 0.8 L/h according to the manufacturer's data, it results in an extraordinary consumption of 3.4 L per day. Consequently, the use of the developed HPRS provides fuel savings of approximately 5.2 L/day.

Furthermore, if, according to the manufacturer's specifications, an average intercity consumption of 12.8 L/hour is considered, an 8-hour working day results in a daily consumption of 48.64 L/day, therefore, the developed HPRS saves 10.7% of fuel.

In summary, assuming that the average annual delivery routes are similar to the test route and that the working week is 5 days, the annual fuel saving is approximately 1,352 L/year (the conversion into money saved will logically be given by the price of diesel in each country; in the case of Spain at the date of the experiment, 2.433 €). This amount of diesel saved, and therefore not burned, means not emitting 3,650 kg of CO_2/year. Of course, from an environmental point of view, not an economic one, the use of the proposed solution only makes sense if the hydrogen used is green, which currently means hydrogen produced by electrolysis from renewable energy sources.

Finally, considering that the investment made in the developed system has been approximately 12,500 euros (this cost would be much cheaper for subsequent units, since a prototype – artisanal– is much more expensive than mass-produced units), it is easy to perform a simple payback analysis of the investment. Savings in diesel fuel is about 3,289.5 €/year. The average consumption of hydrogen is 5.542 Nm^3/day, i.e., about 0.5 kg/day or 130 k/year. Today it is possible to buy green hydrogen between 8 and 10 €/kg; then, considering an average price of 9 €/kg, hydrogen expenditure is 1,170 €/year. Therefore, the approximate payback is slightly<6 years. That said, a system such as the

one developed, industrialized and commercialized, would cost less than half that of the prototype. Add to this the fact that the diesel trend is upward, and the hydrogen trend is downward, the payback would be drastically reduced.

As a conclusion to this discussion section, the design proposed in this work (following the hybridization concept, the design considers the energy balance, not the power balance), although it cannot be considered mathematically optimal, it is probably, based on our experience, one of the most economical and efficient. This is because: (1) the PEMFC always operates at rated power, without any disturbances that could cause it to deteriorate prematurely; (2) the PEMFC is low-power, which means low hydrogen consumption and, therefore, greater autonomy for the cooling system; (3) this translates into less hydrogen to carry on board and therefore less weight in hydrogen cylinders; (4) a small power PEMFC implies a DC/DC converter at its output, also of small power; (5) all these features together lead to a smaller, lighter, more durable and less expensive HPRS. This ensures a quick return on investment.

5. Conclusions

The growth of cities and their suburbs, with the consequent increase in the consumption of goods and food in urban environments, has led to a significant increase in demand in the short-haul transport sector, particularly in the refrigerated food transport sector. Considering that refrigerated delivery vehicles maintain the cold chain using exclusively fossil fuel energy (gasoline/diesel), there is a serious threat to the environment in this field.

In this work, the design, step-by-step development, and experimental validation of a hydrogen-powered refrigeration system (HPRS) for use in refrigerated light trucks for the food delivery sector has been carried out. The main contributions focus on the design of the HPRS architecture, the necessary electronics (acquisition, control, and power supply) for its correct operation, as well as an energy management system (EMS) and a novel algorithm oriented to maximize the performance of the HPRS in terms of operability, power and lifespan.

Focusing on the experimental results obtained on an experimental prototype based on a commercial vehicle, it can be summarized that:

(1) Hydrogen technologies enable the development of technically feasible and safe solutions with zero net emissions for use in the refrigerated food transport sector.
(2) The design philosophy used allows easy integration into the current vehicle fleet, minimizing the economic and research efforts for the promotion and use of hydrogen technologies in the refrigerated food transport sector.
(3) The design of the HPRS and EMS architecture guarantees the required autonomy for use in short-range refrigerated vehicles without refuelling stops.
(4) The use of the developed HPRS presents great advantages in terms of economic savings and environmental care, since, for the vehicle tested, its use allows reducing the average annual fuel consumption by more than 10% and reducing CO_2 emissions by up to 3650 kg.

Future work is oriented in two directions. On the one hand, to try to transfer the developed technology so that refrigerated vans and light trucks that base their cooling systems on the use of hydrogen can begin to be manufactured in series. On the other hand, based on the technology developed, to design HPRS of greater power and autonomy, viable for assembly in heavy refrigerated trucks used in national and international transport. Furthermore, although a cost-sensitive analysis was not within the scope of this work, given current diesel prices (a major problem for the transport sector), it is certainly a challenge for future work.

The pedagogy used in this work and its replicability allows researchers, manufacturers, stakeholders, and policy makers to use it as a starting point for the design of new models or solutions for the existing fleet of refrigerated delivery vehicles, to move towards sustainable mobility and demonstrate the feasibility of using hydrogen technologies.

CRediT authorship contribution statement

F. Segura: Investigation, Conceptualization, Methodology, Writing – original draft. **F.J. Vivas:** Investigation, Conceptualization, Methodology, Formal analysis, Software, Writing – original draft. **J.M. Andújar:** Conceptualization, Writing – review & editing, Project administration, Supervision. **M. Martínez:** .

Declaration of Competing Interest

The authors declare that they have no known competing financial interests or personal relationships that could have appeared to influence the work reported in this paper.

Data availability

No data was used for the research described in the article.

Acknowledgement

This work is a contribution of the two following Projects: “H2Integration&Control. Integration and Control of a hydrogen-based pilot plant in residential applications for energy supply”, Ref. PID2020-116616RB-C31 supported by the Spanish State Program of R + D + I Oriented to the Challenges of Society; and “SALTES: Smartgrid with reconfigurable Architecture for testing controL Techniques and Energy Storage priority contaminant waste”, Ref. P20-00730 supported by Andalusian Regional Program of R + D + I. Funding for open access charge: Universidad de Huelva/CBUA.

References

[1] Kookana RS, Drechsel P, Jamwal P, Vanderzalm J. Urbanisation and emerging economies: issues and potential solutions for water and food security. Sci Total Environ 2020;732:139057. https://doi.org/10.1016/j.scitotenv.2020.139057.
[2] Urbanization - Our World in Data n.d.
[3] Pandya B, El-Kharouf A, Venkataraman V, Steinberger-Wilckens R. Comparative study of solid oxide fuel cell coupled absorption refrigeration system for green and sustainable refrigerated transportation. Appl Therm Eng 2020;179:115597. https://doi.org/10.1016/j.applthermaleng.2020.115597.
[4] MITECO. Gases de efecto invernadero. Serie 1990-2019. Informe resumen 2021: 7–7.
[5] Di Trolio P, Di Giorgio P, Genovese M, Frasci E, Minutillo M. A hybrid power-unit based on a passive fuel cell/battery system for lightweight vehicles. Appl Energy 2020;279:115734. https://doi.org/10.1016/j.apenergy.2020.115734.
[6] Yang Z, Tate JE, Morganti E, Shepherd SP. Real-world CO2 and NOX emissions from refrigerated vans. Sci Total Environ 2021;763:142974. https://doi.org/10.1016/j.scitotenv.2020.142974.
[7] Commission E. CO_2 emission performance standards for cars and vans n.d.
[8] Tassou SA, De-Lille G, Ge YT. Food transport refrigeration - approaches to reduce energy consumption and environmental impacts of road transport. Appl Therm Eng 2009;29:1467–77. https://doi.org/10.1016/j.applthermaleng.2008.06.027.
[9] Garde R, Jiménez F, Larriba T, García G, Aguado M, Martínez M. Development of a fuel cell-based system for refrigerated transport. Energy Procedia 2012;29:201–7. https://doi.org/10.1016/j.egypro.2012.09.025.
[10] Mac KM, Razeghi G, Samuelsen S. The role of fuel cells in port microgrids to support sustainable goods movement. Renew Sustain Energy Rev 2021:147. https://doi.org/10.1016/J.RSER.2021.111226.
[11] Meneghetti A, Dal Magro F, Romagnoli A. Renewable energy penetration in food delivery: coupling photovoltaics with transport refrigerated units. Energy 2021; 232:120994. https://doi.org/10.1016/j.energy.2021.120994.
[12] Union T, Journal O, Union E. Regulation 2019/631 of the European Parliament and of the Council of 17 April 2019 2017;10:1–21.
[13] DGT. No Title; 2019.
[14] Commisiomn E. Assessment of the final national energy and climate plan of Spain. 2020.
[15] Zhuang W, Li (Eben) S, Zhang X, Kum D, Song Z, Yin G, et al. A survey of powertrain configuration studies on hybrid electric vehicles. Appl Energy 2020; 262. https://doi.org/10.1016/j.apenergy.2020.114553.
[16] Mat ZBA, Madya, Kar YB, Hassan SHBA, Talik NAB. Proton exchange membrane (PEM) and solid oxide (SOFC) fuel cell based vehicles-a review. In 2017 2nd IEEE

International Conference on Intelligent Transportation Engineering, ICITE 2017; 2017. p. 123–6. 10.1109/ICITE.2017.8056893.
[17] Venkataraman V, Pacek AW, Steinberger-Wilckens R. Coupling of a solid oxide fuel cell auxiliary power unit with a vapour absorption refrigeration system for refrigerated truck application. Fuel Cells 2016;16:273–93. https://doi.org/10.1002/fuce.201500124.
[18] Yang B, Li Y, Li J, Shu H, Zhao X, Ren Y, et al. Comprehensive summary of solid oxide fuel cell control: a state-of-the-art review 2022;vol. 7. https://doi.org/10.1186/s41601-022-00251-0.
[19] Malik V, Srivastava S, Bhatnagar MK, Vishnoi M. Comparative study and analysis between Solid Oxide Fuel Cells (SOFC) and Proton Exchange Membrane (PEM) fuel cell – a review. Mater Today: Proc 2021;47:2270–5. https://doi.org/10.1016/j.matpr.2021.04.203.
[20] de las Heras A, Vivas FJJ, Segura F, Andújar JMM. How the BoP configuration affects the performance in an air-cooled polymer electrolyte fuel cell. Keys to design the best configuration. Int J Hydrogen Energy 2017;42:12841–55. https://doi.org/10.1016/j.ijhydene.2016.11.051.
[21] Marx N, Hissel D, Harel F, Pahon E, Courteille B, Chaillou F. On the design of a hybrid fuel cell – Battery genset for a refrigerated semi-trailer truck. In 2018 IEEE Vehicle Power and Propulsion Conference, VPPC 2018 – Proceedings; 2019. 10.1109/VPPC.2018.08605015.
[22] Baghzouz Y, Hurt R, Boehm RF. Evaluation of a fuel cell for powering the electrical load of ICE vehicles. In 2007 International Conference on Clean Electrical Power, ICCEP '07; 2007. p. 74–7. 10.1109/ICCEP.2007.384189.
[23] Vivas FJ, de las Heras A, Segura F, Andújar JM. Cell voltage monitoring All-in-One. A new low cost solution to perform degradation analysis on air-cooled polymer electrolyte fuel cells. Int J Hydrogen Energy 2019;44:12842–56. https://doi.org/10.1016/j.ijhydene.2018.12.172.
[24] Marx N, Hissel D, Harel F, Courteille B. Experimental testing of a hydrogen genset used in a refrigerated semi-trailer truck application. In IEEE Vehicle Power and Propulsion Conference (VPPC); 2019. p. 5. 10.1109/VPPC46532.2019.8952231.
[25] PNNL project with Nuvera. Plug power for refrigerated trucks. Fuel Cells Bull 2013; 2013:4. https://doi.org/10.1016/S1464-2859(13)70311-0.
[26] Chang Y, Zhao J, Shahgaldi S, Qin Y, Yin Y, Li X. Modelling of mechanical microstructure changes in the catalyst layer of a polymer electrolyte membrane fuel cell. Int J Hydrogen Energy 2020;45:29904–16. https://doi.org/10.1016/j.ijhydene.2018.10.157.
[27] Calderón AJ, Vivas FJ, Segura F, Andújar JM. Integration of a multi-stack fuel cell system in microgrids: a solution based on model predictive control. Energies 2020: 13. https://doi.org/10.3390/en13184924.
[28] Uddin MN, Nageshkar VV, Asmatulu R. Improving water-splitting efficiency of water electrolysis process via highly conductive nanomaterials at lower voltages. Energy Ecol Environ 2020;5:108–17. https://doi.org/10.1007/s40974-020-00147-5.
[29] Napole C, Derbeli M, Barambones O. A global integral terminal sliding mode control based on a novel reaching law for a proton exchange membrane fuel cell system. Appl Energy 2021;301:117473. https://doi.org/10.1016/j.apenergy.2021.117473.
[30] Andujar JM, Vivas FJ, Segura F, Calderon AJ. Integration of air-cooled multi-stack polymer electrolyte fuel cell systems into renewable microgrids. Int J Electr Power Energy Syst 2022;142:108305. https://doi.org/10.1016/j.ijepes.2022.108305.
[31] Benaggoune K, Yue M, Jemei S, Zerhouni N. A data-driven method for multi-step-ahead prediction and long-term prognostics of proton exchange membrane fuel cell. Appl Energy 2022;313:118835. https://doi.org/10.1016/j.apenergy.2022.118835.
[32] Uno M, Tanaka K. Pt/C catalyst degradation in proton exchange membrane fuel cells due to high-frequency potential cycling induced by switching power converters. J Power Sources 2011;196:9884–9. https://doi.org/10.1016/j.jpowsour.2011.08.030.
[33] Ma T, Yang H, Lu L. Development of hybrid battery-supercapacitor energy storage for remote area renewable energy systems. Appl Energy 2015;153:56–62. https://doi.org/10.1016/j.apenergy.2014.12.008.
[34] Vivas FJ, De Las HA, Segura F, Andújar JM. A review of energy management strategies for renewable hybrid energy systems with hydrogen backup. Renew Sustain Energy Rev 2018;82:126–55. https://doi.org/10.1016/j.rser.2017.09.014.
[35] Enrique JM, Durán E, Sidrach-de-Cardona M, Andújar JM. Theoretical assessment of the maximum power point tracking efficiency of photovoltaic facilities with different converter topologies. Sol Energy 2007;81:31–8. https://doi.org/10.1016/j.solener.2006.06.006.
[36] Enrique JM, Andújar JM, Bohórquez MA. A reliable, fast and low cost maximum power point tracker for photovoltaic applications. Sol Energy 2010;84:79–89. https://doi.org/10.1016/j.solener.2009.10.011.
[37] Collong S, Kouta R. Fault tree analysis of proton exchange membrane fuel cell system safety. Int J Hydrogen Energy 2015;40:8248–60. https://doi.org/10.1016/j.ijhydene.2015.04.101.
[38] Andújar JM, Segura F, Isorna F, Calderón AJ. Comprehensive diagnosis methodology for faults detection and identification, and performance improvement of Air-Cooled Polymer Electrolyte Fuel Cells; 2018. 10.1016/j.rser.2018.02.038.